

NAIST-IS-MT1151132

Master's Thesis

Continuous Estimation of Finger Joint Angles Using Muscle Activation Inputs from Surface EMG Signals

Jimson Gelbolingo Ngeo

March 15, 2013

Department of Information Science
Graduate School of Information Science
Nara Institute of Science and Technology

A Master's Thesis
submitted to Graduate School of Information Science,
Nara Institute of Science and Technology
in partial fulfillment of the requirements for the degree of
MASTER of ENGINEERING

Jimson Gelbolingo Ngeo

Thesis Committee:

Professor Kazushi Ikeda	(Supervisor)
Professor Tsukasa Ogasawara	(Co-supervisor)
Associate Professor Tomohiro Shibata	(Co-supervisor)
Assistant Professor Tomoya Tamei	(Committee)

Continuous Estimation of Finger Joint Angles Using Muscle Activation Inputs from Surface EMG Signals*

Jimson Gelbolingo Ngeo

Abstract

Surface electromyographic (sEMG) signals are often used in many robot and rehabilitation applications because these reflect the motor intentions of users very well. However, inherent problems such as electromechanical delay (EMD) are present in such applications. Many have focused on discrete classification of hand gestures, but natural hand movements are continuous. In this thesis, we present a method to predict multiple finger joint angles from sEMG signals located in the forearm using a so-called EMG-to-Muscle Activation model that parameterizes EMD. An artificial neural network (ANN) and a Gaussian Process (GP) regressor were both evaluated and used to predict joint angles in movements involving individual and simultaneous finger flexion and extension in two subjects. With ANN, results show correlations as large as 0.92 between measured and predicted finger joint angles and an overall average root-mean-square error of 5 to 12%. Using Gaussian Process gave better prediction results specially when using few training samples. Our results also show that predictions improved when the proposed muscle activation input was used compared to using conventional filtered sEMG or time-domain based features used by related studies. Lastly, a dimensionality analysis of hand and finger movements using Principal Component Analysis (PCA) was done. Our results show that the effective dimensionality is much lower than the theoretical 20 degrees-of-freedom available on the hand. This last part may suggest the existence of motor synergies in the control of the hand.

Keywords:

Surface EMG, Artificial Neural Network, Gaussian Process, Finger Joint Angles, PCA

*Master's Thesis, Department of Information Science, Graduate School of Information Science, Nara Institute of Science and Technology, NAIST-IS-MT1151132, March 15, 2013.

Contents

1	Introduction	1
1.1.	Overview of Hand Assistive Devices	2
1.2.	Related Studies	4
1.3.	Motivation and Aim of the Research	5
1.4.	Thesis Overview	5
2	The Biological System of the Hand	6
2.1.	The Bone Structure of the Hand	6
2.2.	Articulations of the Hand	7
2.3.	Hand Movements	10
2.4.	The Brain as the Control System	11
2.5.	Muscles associated to Hand Movements	15
2.5.1	Intrinsic Muscles	15
2.5.2	Extrinsic Muscles	16
3	Surface Electromyographic Signals	19
3.1.	What are Surface Electromyographic Signals?	19
3.1.1	Motor Unit Action Potential	22
3.1.2	Surface EMG Generation	23
3.1.3	The Raw Surface EMG Signal	24
3.1.4	Factors Affecting Surface EMG Signal	24
3.2.	Detecting and Recording Surface EMG Signals	25
3.2.1	Electrodes	25
3.2.2	Signal Amplification and Sampling	27
3.2.3	A/D Conversion and EMG Sampling Rate	27

3.3.	EMG Signal Processing	28
3.3.1	Full-wave Rectification	28
3.3.2	Smoothing	28
3.3.3	Normalization	30
3.4.	Applications of Using sEMG Signals	30
3.5.	Time Domain Features of sEMG Signals	31
4	Continuous Estimation of Finger Joint Angle from Surface EMG	33
4.1.	Problems of Electromechanical Delay	34
4.2.	EMG-to-Muscle Activation Model	35
4.3.	Regression Methods	38
4.3.1	Artificial Neural Network	38
4.3.2	Gaussian Process for Regression	40
5	Experiments	44
5.1.	Experimental Set-up	44
5.2.	Data Collection	47
5.3.	Data Preprocessing	48
6	Results and Analysis	50
6.1.	Prediction of Finger Joint Angles from Muscle Activation Inputs	50
6.2.	Comparison Between Different EMG Features	54
6.3.	Comparison Between ANN and GP Regression	55
6.4.	Dimensionality Analysis for Hand/Finger Movements	57
7	Conclusion	61
Acknowledgements		63
References		65
Appendix		70
A.	Prediction Performance of ANN and GP Regression	70
B.	Processed EMG Used in the Sample Test Result	72
C.	PIP and DIP Joint Angles Prediction Results	73
D.	Application: Control of a Finger Exoskeleton	75

List of Figures

1.1 Examples of hand robot and telemanipulation devices	3
2.1 Bones in the right wrist and hand in palmar view	7
2.2 View of the metacarpal and carpal bones in the right hand	8
2.3 Lateral view of the middle finger	9
2.4 The total degrees of freedom (DOF) available in the hand	9
2.5 Illustration of a sample joint coordinate system in the hand	10
2.6 The motor cortex in the brain	11
2.7 Activation sequence for the motor areas	13
2.8 Neural control information are sent from the brain	14
2.9 The motor homunculus by Penfield	14
2.10 Intrinsic muscles of the hand	16
2.11 Extrinsic muscles of the hand	18
3.1 Illustration of the depolarization and repolarization cycle	20
3.2 The action potential	21
3.3 Recruitment of motor units and its firing frequency	22
3.4 Overview of the generation of sEMG signal	23
3.5 A sample raw EMG recording of 3 contraction bursts	24
3.6 Regular EMG/ECG electrodes by AMBU-Blue Sensors	26
3.7 Different stages of the preprocessing part of the sEMG	29
4.1 The electromechanical delay is shown	34
4.2 The parameter A introduces nonlinearity	37
4.3 A sample raw EMG recording is low-pass filtered	37
4.4 The architecture of a feedforward artificial neural network.	39

5.1	Electrode placement was based on muscle locations	44
5.2	The wireless sEMG device is based on a BA1104	45
5.3	The motion camera system set-up	46
5.4	Twenty-two reflective markers are attached on the joints	46
5.5	A screen capture showing the subject's hand	47
6.1	Single joint angle prediction results	51
6.2	Index finger joint angle estimation for a flexion motion	52
6.3	Index finger joint angle estimation for a free hand motion.	53
6.4	The mean correlation coefficient	54
6.5	The mean normalized root-mean-square error (NRMSE)	55
6.6	Learning curves of the neural network and Gaussian process	56
6.7	The predicted MCP joint angles trained with 214 samples	57
6.8	The predicted MCP joint angles trained with 2134 samples	57
6.9	PCA on the finger joint angle data	59
6.10	PCA on the finger joint velocity data	60
7.1	Prediction Performance of the ANN and GP Regressor	71
7.2	Muscle activations are transformed from preprocessed EMG	72
7.3	The actual and predicted PIP joint angles	73
7.4	The actual and predicted DIP joint angles	74
7.5	An application showing an sEMG-based control of an index finger exoskeleton	75

List of Tables

2.1	Flexor muscles	17
2.2	Extensor muscles	17
5.1	Selected EMG channels and the target muscles	45
5.2	Finger joints normal range of motion	49
6.1	Muscle activation model parameters	52

Chapter 1

Introduction

In the coming years, human assistive and tele-manipulation technologies are expected to play a significant role in improving the lives and well-being of the ageing community and as well as the handicapped and injured. This predicted growth in assistive technology will be driven by the need to enhance functional independence and support among them. For instance, assistive robotic devices and brain-machine interfaces are developing technologies that have the potential to give tireless support, enabling persons with impairments and injuries to achieve more function and mobility.

Given the dominant role of the human hand, where many everyday functional tasks such as touch, grasp, manipulation and communication are achieved by our hands, the loss of hand function can greatly affect daily human functions and mobility. Hand exoskeletons, rehabilitation aids, and robot prosthetics are some common solution for rehabilitating impaired or injured hands, and even possibly for replacing upper limb loss. Thus, providing a means to accurately replicate refine hand motions can greatly improve current support devices, particularly, in the development of devices and applications, such as hand and finger exoskeletons, that can aid in hand rehabilitation.

This thesis has the main goal of creating a system that can perceive a person's will to move his hands and fingers through the use of surface electromyograph (sEMG), and translating these signals into useful finger kinematic information which can be used in the study of hand biomechanics and also in the control of hand assistive devices.

Surface electromyographic signal based control is widely used in prosthetic devices and in clinical rehabilitation applications. In any body movements produced by exerted tensions, electromyographic (EMG) signals are read and recorded by attaching surface

electrodes on top of the exerting muscles. It is because of this close relationship that the EMG and the exerted movement has, that we use EMG in trying to asynchronously decode continuous hand kinematic information such as finger joint angles.

Many studies have been done on using EMG signals, but a majority of the effort have focused on decoding discrete hand movements and discriminating a limited set of hand gestures. Since natural hand movement is continuous and the number of possible variations in movements is infinite, our work focuses on predicting continuous finger joint angles from sEMG signal inputs.

We show some inherent problems encountered in such sEMG to motion applications and investigate different types of sEMG features to determine which are best suitable in predicting continuous hand motions. We also explore the use different machine learning regression techniques such as artificial neural network and nonparametric Gaussian process regression in predicting finger joint angles coming from a user's sEMG signal.

1.1. Overview of Hand Assistive Devices

Robotic hand assistive devices and telemanipulation devices are developing technologies that hold great promise in revolutionizing modern hand rehabilitation and prosthetic applications. Robotic systems for rehabilitation can focus on providing missing movements and sensing, and providing environments that make regaining movement-related function easier and faster [1]. Robotic hand prosthetics and exoskeletons on the other hand can provide hand functionality, dexterity, and mobility to missing or paralyzed hands. Also telemanipulation and haptics devices such as those used in virtual reality applications have found a niche in developing new man-machine interfaces that do not require explicit interaction with a physical device in the hand but rather using only the sole intent of moving one's hands.

Much focus is given on returning and rehabilitating hand functionality because of the immense importance that the hands play in doing daily life activities. The hand is a complex biological system with many joints and muscles, and can perform many complex manipulation tasks. That is why being able restore and improve hand function by means of replicating hand motion either through robotic supports or human interfaces can greatly improve current support devices.

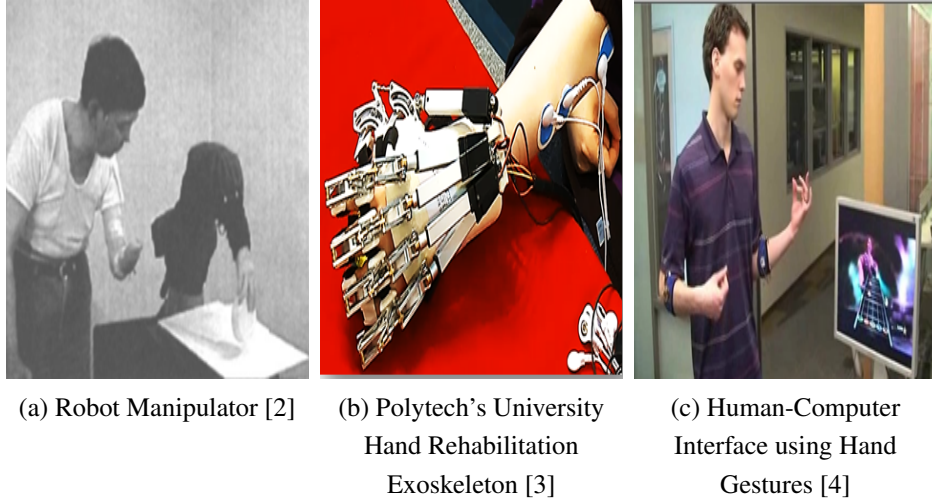


Figure 1.1: Examples of hand robot and telemanipulation devices that makes use of a user’s own myographic signal.

Presently, there are existing robotic devices and rehabilitation aids that can support hand and finger functionality and rehabilitation (see Figure 1.1). Figure 1.1a shows a robot manipulator being controlled by a transradial amputee. Such a manipulator system has been shown that it could assist amputees perform some basic desktop work such as pointing, touching and grasping objects [2]. In Figure 1.1b is a recently made hand rehabilitation exoskeleton by Hong Kong’s Polytech University. This device is made for patients with hand impairments or those recovering from stroke to wear, to assist them in doing simple hand opening and closing functional tasks. Figure 1.1c shows a muscle-computer interface from sEMG signals made by Microsoft Research that allows a user to play the Guitar Hero game. Typically in a game like Guitar Hero, users hold a guitar-like controller, but with the muscle-computer interface, the user can play without the guitar as the muscle signals are classified to determine hand and finger gestures. Such an interface has a good impact in applications where users either cannot or prefer not to explicitly interact with a physical device in hand.

What is common in all the devices shown aside from being able to replace, support, and assist hand functionality is that all the devices are driven by myographic signals. In other words, the devices were controlled by the user’s own muscle signals via the use of surface electromyography (sEMG) sensors attached on to the patient’s arm.

Surface electromyographic signal based control is widely used in prosthetic devices and in clinical rehabilitation applications primarily because of its non-invasive nature. SEMG signals are stochastic electrical signals produced during muscle contraction when nerve impulses are sent by motor neurons in the brain down to the muscle fibers.

1.2. Related Studies

Many works have been carried out in this field where sEMG signals have been used in many different applications. However, many of these studies have focused on discriminating a limited set of hand gestures and the control schemes of many such devices and interfaces still remain somewhat unnatural. So in this thesis, rather than focusing on decoding a discrete set of hand movements, we focus on continuously decoding finger joint angles from sEMG signals extracted from the hand.

Related studies have shown that it is possible to extract fine finger movement information contained in sEMG signals. Afshar and Matsuoka [5] were able to estimate the index finger joint angles from fine-wire EMG embedded inside seven muscles that control the index finger. Similarly, Shirrao et al. [6] were able to decode one index finger joint angle from surface EMG signals. The types of finger motion involved in their study were periodic flexion-extension movements of the index finger at three different frequencies (low, medium, and high speed) of motion. In their study, they used and evaluated different committees of neural network to predict the joint angle.

In a more recent development, Smith et al. [7] were able to asynchronously decode individual metacarpophalangeal (MCP) joint angles of all five fingers while moving one finger at a time. Their study used general placement of electrodes in muscle areas available to transradial amputees and extracted sEMG time-domain features used as input to a feed-forward neural network to predict the MCP joint angles. Hioki et al. [8] predicted all finger joint angles using only 4 sEMG channels and a recurrent neural network with time delay parameters. However, their method requires too many parameters which makes it difficult to optimize and implement across different subjects.

1.3. Motivation and Aim of the Research

However in many of the previous cited studies [6][7], a time delay between the onset of the sEMG signal and exerted movement was present and observed. This time delay is called hysteresis or electromechanical delay (EMD). It is often compensated by either manually realigning the sEMG to the joint angle data before any processing is done or by introducing time-delay lines, making use of all the immediate and past values of the sEMG which can greatly increases the number of inputs and as well as parameters of the predictor. EMD can vary depending on many different factors such as muscle shortening velocity, type of muscle fiber, and fatigue[6]. In our method, we introduce this delay as a parameter, by using an EMG-to-Muscle Activation Model, which is determined along with other parameters through optimization.

Very few studies have also studied and predicted more than 5 finger joint angles from EMG signals. In this thesis, we investigate the use of muscle activation as input to a regressor in predicting continuous flexion and extension movement of all fifteen finger joint angles simultaneously. We attempt to predict the angular position of each finger joint, namely, the metacarpophalangeal (MCP), proximal interphalangael (PIP) and the distal interphalangeal (DIP) joints.

1.4. Thesis Overview

This thesis is organized and divided into seven chapters. Chapter 2 introduces the anatomical system and biomechanical function of the hand. While, chapter 3 gives the concepts behind surface electromyographic signal generation and its usage. Chapter 4 discusses the method that we used in the continuous estimation of finger joint angles from sEMG signals. We discussed several features of sEMG signals and the regression techniques used. Chapter 5 explains the experimental set-up, data collection from subjects and data pre-processing. Chapter 6 presents the results and performance of the finger joint angle predictors using EMG signals and as well as include basic statistics and dimensionality analysis of hand movements. Lastly, Chapter 7 draws some conclusions and gives some perspectives to applications for future expansion of the current work.

Chapter 2

The Biological System of the Hand

The upper limb consists of three main parts: the arm, forearm and the hand. The arm is composed of the shoulder down to the elbow. While the forearm is composed of the portion from the elbow down to the wrist. The last part, which is the hand, which will be the primary focus of this research, consists of the remaining parts down from the forearm, which includes the palm and digits (or fingers).

Hand anatomy is very complex because it consists of so many muscles and joints. It can also assume a huge variety of positions and range of motion that allows the hand to perform numerous functions and manipulations [9].

2.1. The Bone Structure of the Hand

The bones of the hand form the basic framework that defines the overall shape and serves as a stable base for soft tissues in the hand. There are 19 major bones in the hand, which mainly consists of two types: the metacarpals and the phalanges (see Figure 2.1). All of these bones are classified as long bones and are arranged to maximize functional efficiency of the muscles and tendons in the hand [9].

Each *metacarpal* is associated with each finger, with the one on the thumb relatively shorter than the rest. The metacarpals have closely positioned bases but diverges in distance to the hands. This arrangement determines the shape of the hand and separates the digits so they can function independently [9]. In the case of the thumb, its metacarpal is anterior and is rotated approximately 90 degrees which creates opposing movements compared to the other fingers.

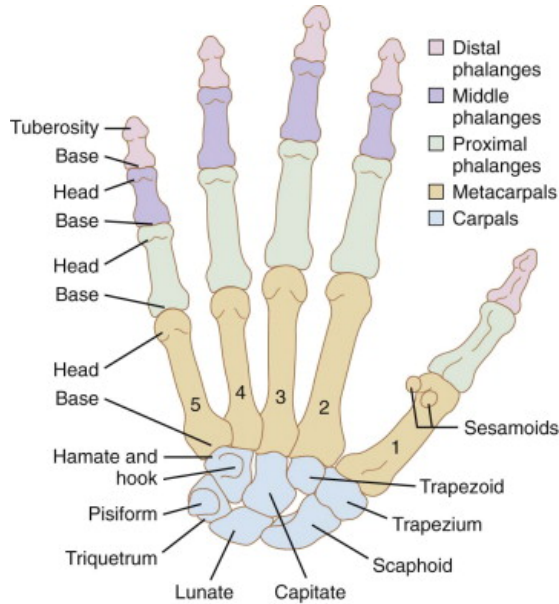


Figure 2.1: Bones in the right wrist and hand in palmar view [9]

As for the *phalanges*, there are about 14 in the hand. Each finger has three phalanges, with the exception of the thumb which only has two. The *proximal* and *distal* have bowed dorsal shapes which are similar to the metacarpals. Its body are cylindrical in shape, but the sides are marked by rough edges which serve as anchors for different fibrous sheath of digital flexor tendons.

2.2. Articulations of the Hand

The *carpometacarpal (CMC) joints* are the most proximal joints which connect the hand digits or fingers to the wrist. The thumb CMC joint is significantly different from those of the other digits as it can allow more complex and greater range of motion. The CMC joints of the other digits on the other hand can allow only a small amount of restricted movement and sometimes no movement at all.

The *four medial joints* are between the bases of the four metacarpals and the distal row of the carpal bones, which are labeled in Figure 2.1, as the hammate, capitate, trapezoid, and trapezium. The movements permitted at these joints are minimal. No movements are permitted at the CMC joints of the index and middle fingers while only

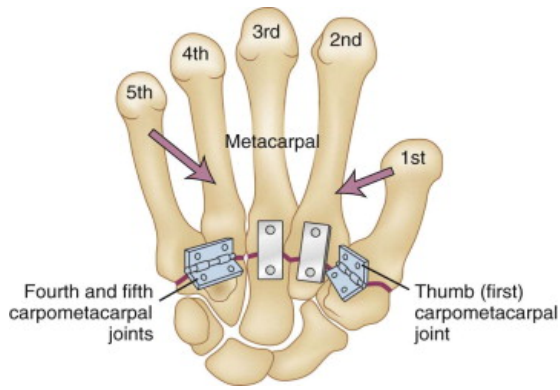


Figure 2.2: View of the metacarpal and carpal bones in the right hand [9]

a small amount of movement are permitted at the CMC joints of the ring and little finger.

The *CMC joint of the thumb* or the *trapeziometacarpal joint* has greater degrees of freedom in movement than the other finger's CMC joint because of the shallow saddle shape of the Trapezium. The movements permitted by this joint are the flexion and extension (where the thumb moves across the palm), abduction and adduction (where the thumb away and towards the index finger, respectively), and pronation and supination (or opposition and retroposition).

The *metacarpophalangeal (MCP) joints* are formed by the bases of the proximal phalanges and the heads of the metacarpals (see Figure 2.2). The articular surface of this joint's base is biconcave, shallow and smaller in area than the head of the metacarpal. The shapes of the phalanges seem to permit movement in any plane on the metacarpal head. However, due to soft tissue restraints, active motion is limited to flexion and extension, and abduction and adduction (movement of the fingers away and towards the middle finger, respectively). As for the thumb MCP joint, movement directions are similar to the other finger's MCP joints, but the flexion and extension movement are less free, and the abduction and adduction are significantly more limited.

The *proximal interphalangeal (PIP) joints* are formed by the head of the proximal phalanges and the base of the middle phalanx. The movements allowed by these joints are only flexion and extension movement. The amount of flexion is significantly considerable, while the extension is very limited.

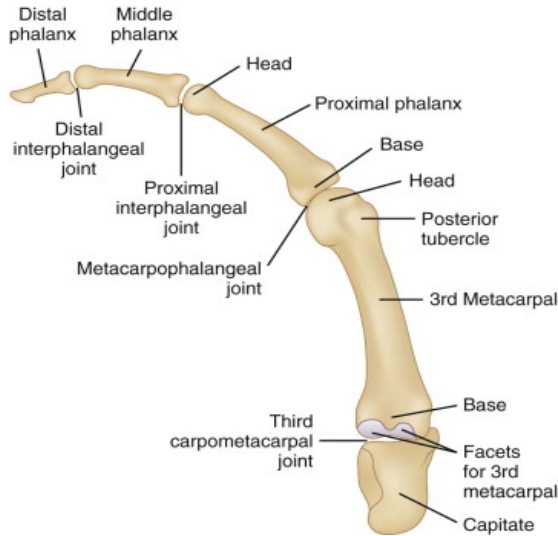


Figure 2.3: Lateral view of the middle finger [9]

The *distal interphalangeal (DIP) joints* are formed by the head of the middle phalanges and the base of the distal phalanx. The movements allowed are the same as the PIP joints but are more limited in angular range of movement.

Overall, the total degrees of freedom (DOF) available on the hand including the wrist is 31 as shown in Figure 2.4. Four for each finger coming from the MCP, PIP, and DIP joints. Five for the thumb coming from the MCP and PIP joints. Four more from the CMC joints and finally, 6 for the wrist which includes rotation and translation movement of the wrists.

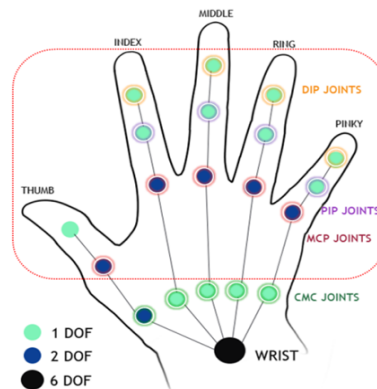


Figure 2.4: The total degrees of freedom (DOF) available in the hand [9]

2.3. Hand Movements

The central focus of this research involves mainly about finger movement. In this section we discuss the different types of movement possible for the human fingers, some of which have already been mentioned in the earlier sections of the chapter.

There are two main types of rotation coordinate commonly used to describe the rotation of a joint. These are the Euler rotations and the Joint Coordinate rotation system. In the Euler rotation system, the axes of rotation are fixed in the object to be rotated. This means that as the object rotates, the orthogonal axes of rotation also rotate. On the other hand, the joint coordinate axes remain invariant as the object rotates. For this research, we solely use the joint coordinate system to describe finger rotation movements.

As an example, we show different types of finger rotations in a sample joint coordinate system with x, y, and z axis defined as shown in Figure 2.5. The figure shows a sample joint coordinate system for the MCP joint on the right hand. The x-axis runs approximately from the index finger to the little finger, the y-axis runs down the center of the finger and the z-axis is normal to the XY plane.

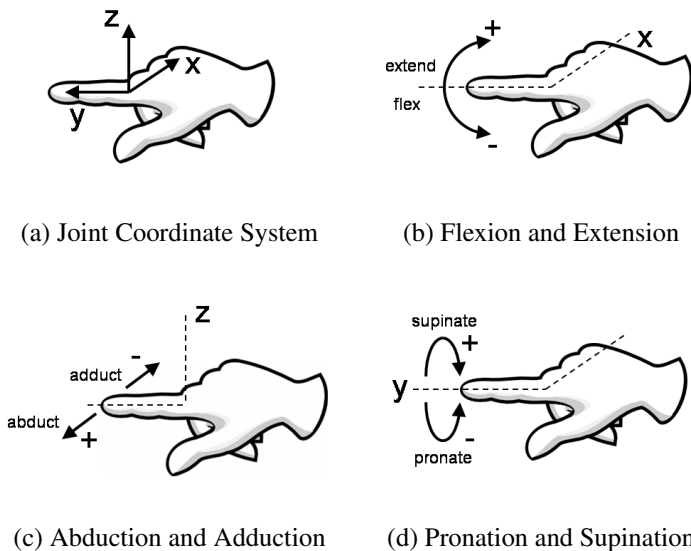


Figure 2.5: Illustration of a sample joint coordinate system in the hand and different finger rotations.

As shown in (b) of Figure 2.5, rotation about the x-axis results in the flexion and extension of the finger. Finger flexion is best described when the fingers curl up to form a fist, while extension is described by the uncurling of the fingers towards opening the palm of the hand. In (c), rotation about the z-axis results in finger abduction or adduction movement. Abduction is best described by the finger moving away from the other fingers, while adduction moves the finger towards the other fingers. Finally in (d), rotation about the y-axis results in pronation or supination of the finger. Pronation is described as a rotation from palm-up to palm-down (with elbow at 90 degrees), while supination is a rotation from palm-down to palm-up.

2.4. The Brain as the Control System

All of the body's movements are controlled by the brain. In fact, the motor cortex is the region in the brain devoted in planning, control, and execution of all voluntary motor functions. It is situated in the rear portion of the frontal lobe and is divided into two main areas, *Area 4* or the *primary motor cortex* and *Area 6* which consists of the *premotor area* and the *supplementary motor area* (see Figure 2.6).

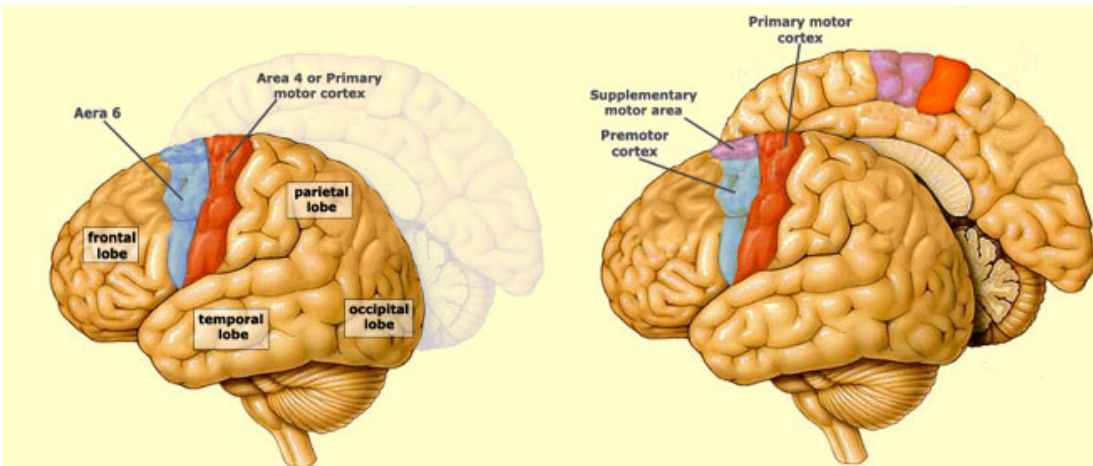


Figure 2.6: The motor cortex in the brain [10].

The regions of the motor cortex and its functions can be organized as follows:

- The Primary Motor Cortex - is said to contain somatotopic representations of different parts of the body. Stimulating this part of the brain have been shown to trigger highly localized muscle contractions on corresponding body parts.
- The Premotor Area (PMA) - is located in the lateral part of Area 6 and is said to help guide body movements by integrating sensory information, and it also helps control the muscles that are closest to the body's main axis.
- The Supplementary Motor Area (SMA) - is located in the medial part of Area 6 and is involved in planning complex movements and in coordinating movements involving both hands.

However, aside from the primary motor cortex, PMA, and SMA, other parts of the brain are also involved in the generation of voluntary movement process. These are summarized as follows:

- The Posterior Parietal Cortex - is located in the parietal lobe and has the function of receiving somatosensory, proprioceptive, and visual inputs, then uses them to determine such things as the positions of the body and the target in space [10]. It thereby produces internal models of the movement to be made, prior to the involvement of the premotor and motor cortex.
- The Basal Ganglia - plays an indirect role in the motor system. Different structures of the basal ganglia form various internal loops that modulate the activity of the main loop, in which information passes through the motor cortex, the PMA, and the SMA. The cortobasal ganglia motor loop, and plays a very important role in determining and controlling what movements are performed.
- The Cerebellum - for the body to make any given gesture, the sequence and duration of each of the basic movements of each body segment involved must be controlled in a very precise manner. One of the cerebellum's jobs is to provide this control over the timing of the body's movements. It does so by means of a loop circuit that connects it to the motor cortex and modulates the signals that the motor cortex sends to the motor neurons.

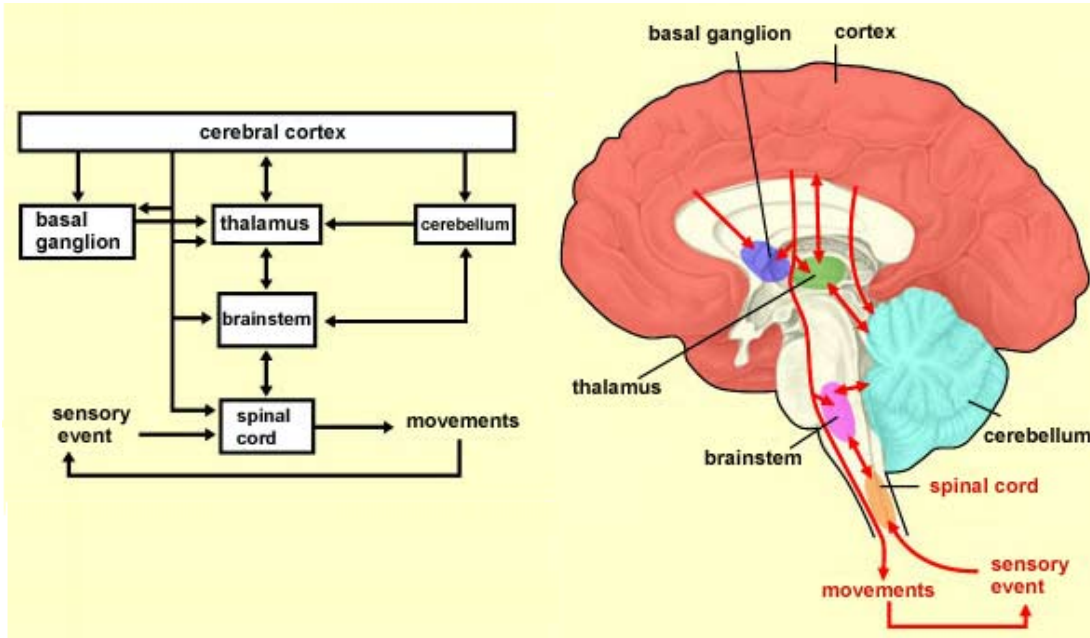


Figure 2.7: Activation sequence for the motor areas [10].

The information processing that the brain must perform to initiate a voluntary movement is hierarchical in nature and can be organized into three steps. The first step is to select an appropriate response to the current situation. The second step is to plan the movement in the physical terms by defining the sequence of muscle contractions required to carry it out the task. Finally, the third step is to execute the movement.

The activation sequence for the motor area in the brain is shown in Figure 2.7. The control messages issued by the motor cortex are themselves triggered by messages from other cortical areas. The motor cortex also communicates closely with subcortical structures such as the basal ganglia and the cerebellum, through the thalamus, which acts as a relay.

Once the movement plan has been established, motor neurons are sent from the primary motor cortex, down to the spinal cord, activating the muscles to produce the necessary contractions and force needed for the movement task (see Figure 2.8). The primary motor cortex, through the motor neurons, determines how much force each muscle group must exert and sends this information down to the muscles for them to actuate different joints in the body to generate the planned movement.

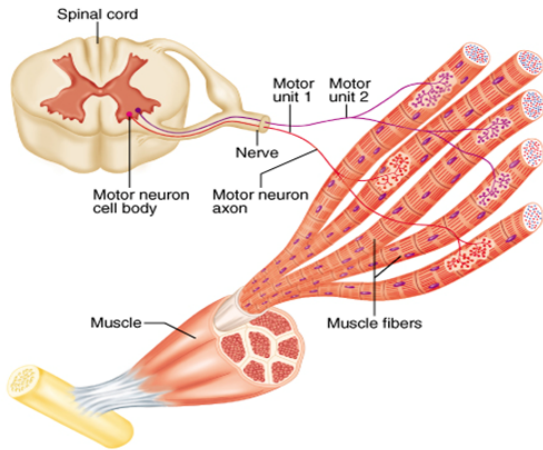


Figure 2.8: Neural control information are sent from the brain to the muscles[11].

In relation to doing hand movements, let's go back to the function of motor cortex and try to see a general view of how the hands are controlled. Dr. Wilder Penfield, while performing operations to alleviate patients' epileptic symptoms, stimulated various areas of the cortex to identify vital ones that should not be removed. In the process, this enabled him to develop a complete map of the motor cortex, known as the motor homunculus as shown in Figure 2.9.

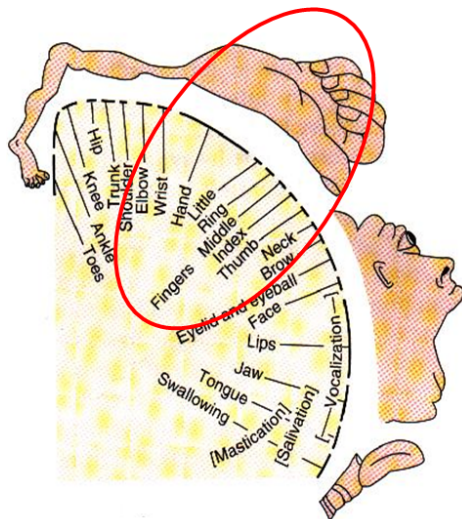


Figure 2.9: The motor homunculus by Penfield [12].

The motor homunculus map shows the amount of muscular control the motor cortex devotes to controlling corresponding body part. It is interesting to see that in this map, the areas assigned to various body parts on the cortex are proportional not to their size, but rather to the complexity of the movements that they can perform. Especially for the hand, almost a quarter of the brain's motor cortex is devoted to moving the hand. This is no surprise, as the hands can perform very complex tasks with speed, dexterity and great precision.

2.5. Muscles associated to Hand Movements

The muscle is a soft and a contractile tissue in the body that generates force. In the movement of any joints, muscles are the main actuators. The muscles in general are connected to the bones via fibrous tissues called tendons. When the muscles related to a certain joint contract the tendons move to actuate the joint.

The muscles moving the human hand can be divided in two groups: the intrinsic and the extrinsic muscles. The former are located within the palm, while the latter are the long flexor and extensors located in the forearm.

2.5.1 Intrinsic Muscles

The intrinsic muscles are those small muscles that both arise and insert within the hand and generally are involved in the finer movements of the digits. They are divided into four groups: the thenar, hypotenar, lumbrical and the interossei group.

The thenar group controls the thumb movements and is located on the radial side. This group is composed of the abductor pollicis brevis, flexor pollicis brevis, and the opponens pollicis. These particularly control thumb abduction, thumb metacarpal and proximal phalanx flexion, and metacarpal opposition movements.

The hypotenar group controls the little finger and is situated on the ulnar side. This group is composed of the abductor digiti minimi, flexor digiti minimi, and opponens digiti minimi. These are all innervated by the ulnar nerve and are responsible for abduction, flexion at the MCP joint, and slight rotation of the little finger.

The lumbrical group contributes to the flexion of the MCP joints and to the extension of both the PIP and DIP joints. Muscles in this group arises from the flexor

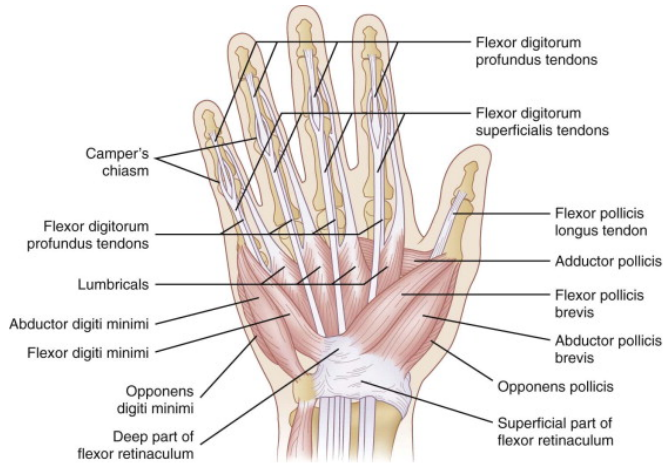


Figure 2.10: Intrinsic muscles of the hand [9].

digitorum profundus tendon on its ulnar side or from both tendons between which the muscles are positioned. The innervation of index and long finger lumbrical muscles are supplied by the median nerve, while the small and ring finger lumbricals are supplied by the ulnar nerve.

The interossei group consists of 3 volar and 4 dorsal muscles, which are all innervated by the ulnar nerve. The volar interossei muscles are responsible for finger adduction movements, while the dorsal muscles abduct the fingers to the hand axis.

Though fine finger movements such as abduction and adduction movements are done by intrinsic muscles in the hand, many of these muscles are relatively small in size and located deep inside the palm. Accessing these muscles may require a more invasive approach or the use of highly localized electrodes. As such, in this research, no surface EMG signals were taken from any intrinsic muscles and the targets were only on selected extrinsic muscles of the hands. We relied that some movement information contained in the intrinsic muscles are embedded in the EMG signals coming from the extrinsic muscles.

2.5.2 Extrinsic Muscles

The extrinsic muscles of the hand are those muscles that arise in the forearm and insert within the hand. These muscles, the long digital flexors and extensors, have muscle bellies located within the forearm and long tendons that cross the wrist and fingers.

Table 2.1: Flexor Muscles

Muscles	Group	Side	Function
Flexor carpi radialis	Superficial	Anterior	Flex. of the hand and wrist
Flexor carpi ulnaris	Superficial	Anterior	:
Palmaris longus	Superficial	Anterior	:
Flexor digitorum superficialis	Intermediate	Anterior	Flex. of 2-5th fingers
Flexor digitorum profundus	Deep	Anterior	:
Flexor pollicis longus	Deep	Anterior	:

Table 2.2: Extensor Muscles

Muscles	Group	Side	Function
Extensor carpi radialis longus	Superficial	Posterior	Ext. of the hand and wrist
Extensor carpi radialis brevis	Superficial	Posterior	:
Extensor carpi ulnaris	Superficial	Posterior	:
Extensor digitorum	Superficial	Posterior	Ext. of 2-5th fingers
Extensor indicis	Deep	Posterior	:
Extensor digiti minimi	Superficial	Posterior	:
Abductor pollicis longus	Deep	Posterior	Ext. and abd. of the thumb
Extensor pollicis brevis	Deep	Posterior	:
Extensor pollicis longus	Deep	Posterior	:

The forearm muscle structure can be organized into the anterior and the posterior compartments. The anterior side of the hand is the side of the hand that people can see when it is supine or the front side view when following an anatomical posture. The anterior compartment contains the flexor muscle, while the posterior compartment contains the extensor muscles.

The flexor muscles found in the forearm are listed in Table 2.1. They can be categorized either superficial, intermediate, or deep muscles depending on the muscle depth starting from the skin surface. The flexor digitorum superficialis actuates the PIP joint, while the flexor digitorum profundus actuates the DIP joint. It is difficult to get proper

signals from the deep muscles. Thus, the prediction or analysis of motion of DIP joint becomes more difficult.

The extensor muscles on the other hand are found on the dorsal side of the arm and are listed in Table 2.2. Similarly with the flexor muscles, they can be categorized either superficial, intermediate, or deep muscles. The extensor digitorum moves the middle and the ring finger, while the extensor indicis and the extensor digiti minimi controls the index and little finger, respectively. These muscles connect to the middle and the distal phalanges and control the movements both for the PIP and DIP joints. Thus, the movements of the PIP and the DIP joint are in some way coupled due to this shared muscle function. Unlike the other fingers, the thumb has more degrees of freedom, and is reflected by the fact that there are more muscles available which functions to control movements of the thumb than in other fingers.

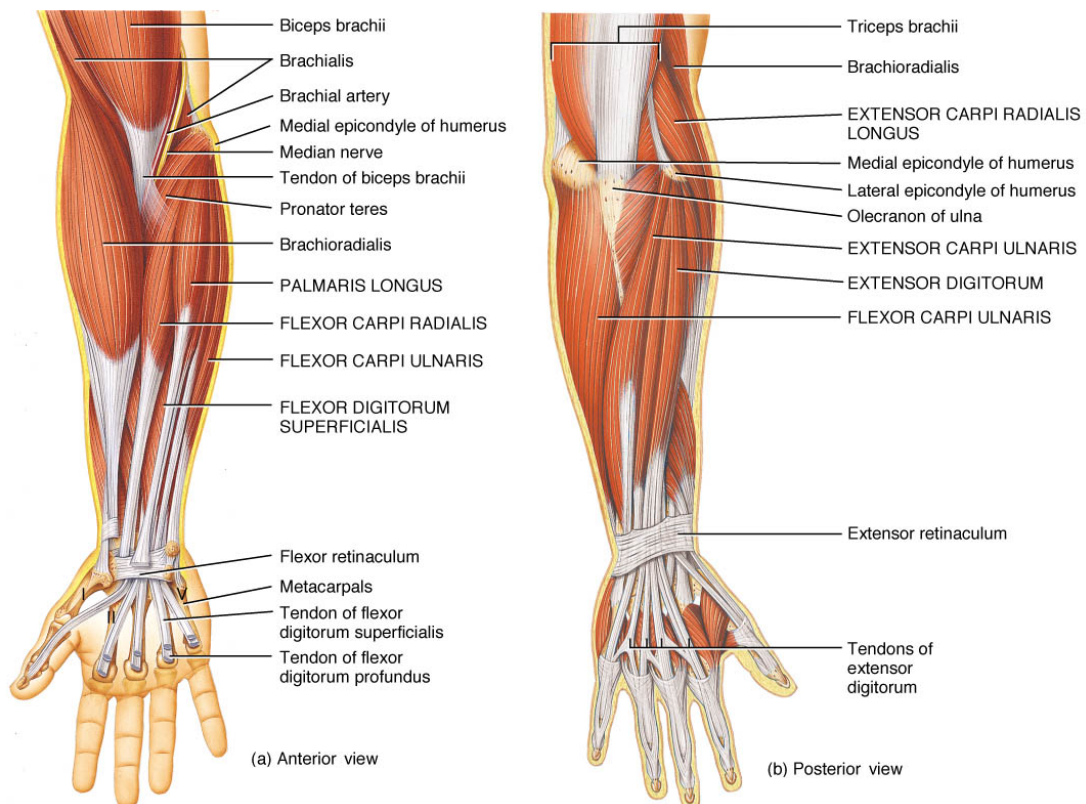


Figure 2.11: Extrinsic muscles of the hand [9].

Chapter 3

Surface Electromyographic Signals

Tele-operated devices controlled by neural signals can give unconstrained and precise movement control in different environments [5]. Surface electromyogram (sEMG) signals are often used in prosthesis controls and rehabilitation support applications because these signals provide an easy and non-invasive access to physiological process that cause muscles to contract [13]. SEMG signals not only provide little delay when used in human interfaces, but have also been shown to represent muscle tension and joint positions very well.

3.1. What are Surface Electromyographic Signals?

Basmijian and De Luca described *electromyography* or more commonly known as *EMG* as an experimental technique concerned with the development, recording, and analysis of myoelectric signals. Myoelectric signals are formed by physiological variations in the state of muscle fiber membranes [14].

As was discussed in Chapter 2.4, movement planning is done by the brain after integration of all sensory information. Motor commands are then generated and transmitted to the muscles by means of motor neurons (also called alpha-motor neurons) located in the spinal cord or brainstem. These motor neurons travel to the muscle fibers, where it then branches out. Due to this branching, each axon in a nerve innervates several muscle fibers which causes the muscles to contract.

A motor neuron along with associated muscle fibers is considered to be the smallest functional unit of the neural control of the muscles and is defined as a *motor unit*. The

term *unit* outlines the behavior, that all muscle fibers of a given motor command act as one unit block in the innervation process [15]. Feinstein et. al. described that one motor unit controls between 3 to 2000 muscle fibers, depending on the refined fineness of control [16].

Accordingly, the excitation of muscle fibers through neural control represents a major factor in muscle physiology. Muscle fibers have a resting potential, such as when the neuron is not transmitting, differing between -80 to -90 mV. This is explained by muscle membrane phenomenon that neurons produce negative ions inside and positive ions outside of the cell membrane. The difference causes an electrical potential across the membrane even when the neuron is not transmitting impulses to stimulate muscle fibers. During muscle fiber innervation, the diffusion characteristics of the muscle fiber membrane are briefly modified and Na^+ ions flow in. This causes a membrane *Depolarization* which is immediately restored by backward exchange of ions within the active physiological process, which is called *Repolarization*. This depolarization and repolarization process is shown in Figure 3.1.

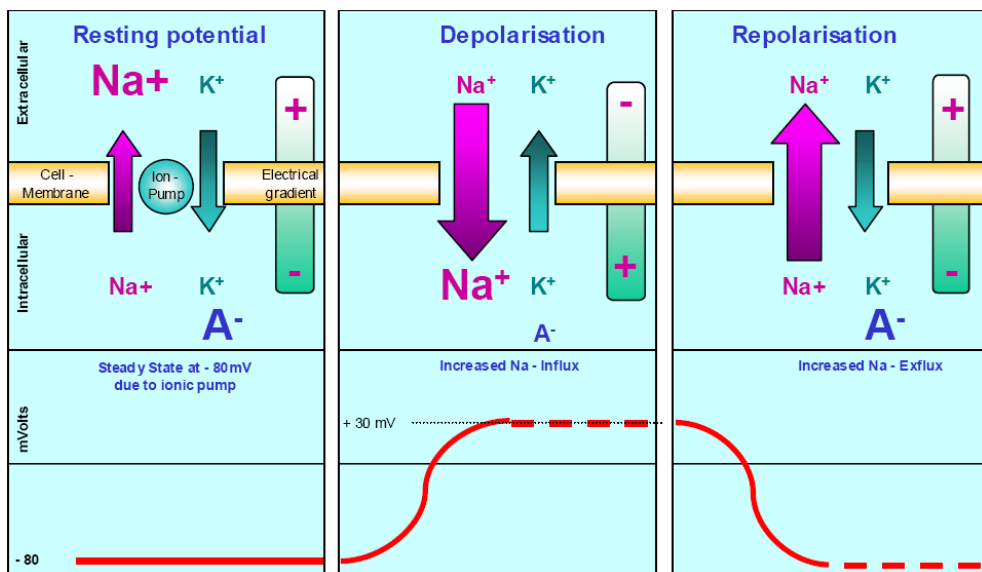


Figure 3.1: Illustration of the depolarization and repolarization cycle in muscle membrane excitation [15].

Because of the membrane depolarization and repolarization process, the movement of ions generate a magnetic field in the neighboring muscle fibers. If a certain threshold level is exceeded within the Na^+ influx in the depolarization process, this causes an *action potential* to quickly change from -80 mV up to $+30 \text{ mV}$ as shown in Figure 3.2. An action potential is a monopolar electrical burst that is immediately restored by repolarization and followed by an after hyperpolarization period in the muscle membrane.

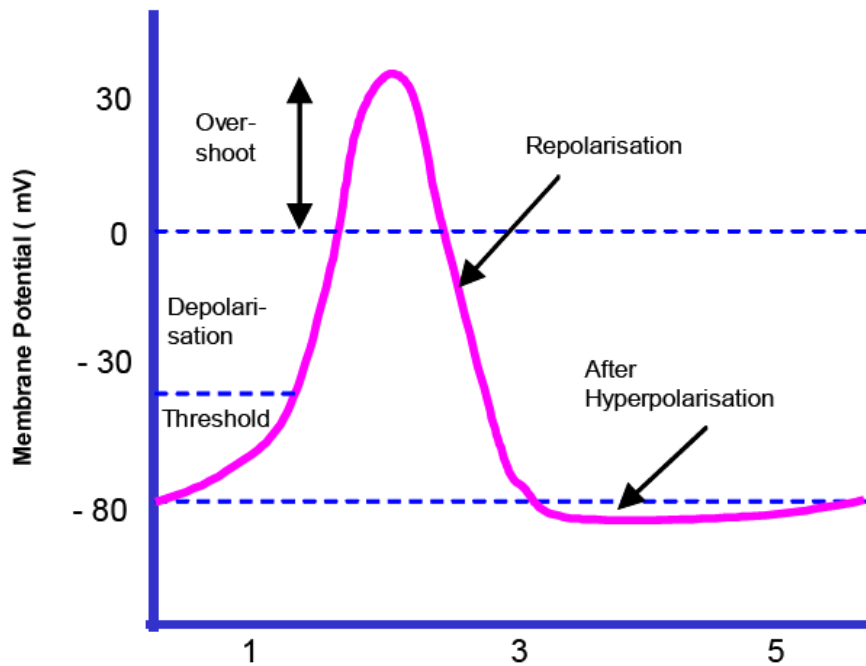


Figure 3.2: The action potential [15].

The EMG signal is based upon the action potential at the muscle fiber. The reading of the amplitude of the action potential is highly dependent on the placed electrode position on the surface on top of the target muscle. Its amplitude is said to be directly proportional to the diameter of the muscle fiber and inversely proportional to the distance between the muscle fiber and the electrode position. Also, the time interval between the generation of the action potential and the detection at the electrode highly depends on the conduction speed of the muscle fiber which ranges from 3 to 6 m/s [15].

3.1.1 Motor Unit Action Potential

The combined or sum of the action potentials of all muscle fibers belonging to a single motor unit is called the *motor unit action potential* or *MUAP*. This combined action potential are typically detected and observed by means of electrodes. Because the target electrode consist of many muscle fibers, the motor unit action potentials across different motor units are electrically superposed and are observed as a bipolar signal with symmetric distribution of positive and negative values. The repetitive firing of a motor unit creates a train of impulses known as the *motor unit action potential train* (*MUAPT*).

There are two main factors that influence the magnitude and density of the observed signal, the recruitment of MUAPs and the firing frequency. These factors determine and modulate the force output at the muscles. Because the human connective tissue and skin layers have a low pass filter effect on the original signal, the analyzed firing frequency of the surface EMG signal does not represent the original firing and amplitude characteristics.

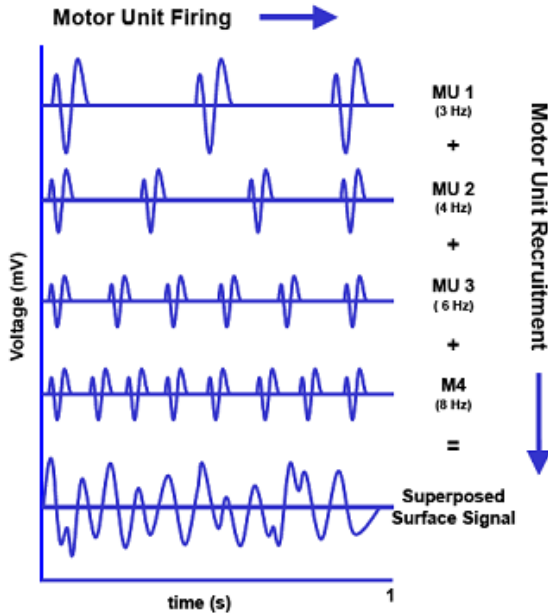


Figure 3.3: Recruitment of motor units and its firing frequency modulates the EMG signal [15].

3.1.2 Surface EMG Generation

An overview of the process of the surface EMG signal generation from the signal coming from the spinal cord down to the target muscle is shown in Figure 3.4. As mentioned earlier, EMG signal directly reflects the recruitment and firing characteristics of the detected motor units within the measured muscle. In the figure, multipath interference of the EMG refers to the spatial and temporal interaction of the MUAPTs generated by all the active motor units in the area of the electrode position [17].

The raw sEMG signal is also shown as a stochastic process, which means that noise and other interference and signal contamination may also superimpose with the signal.

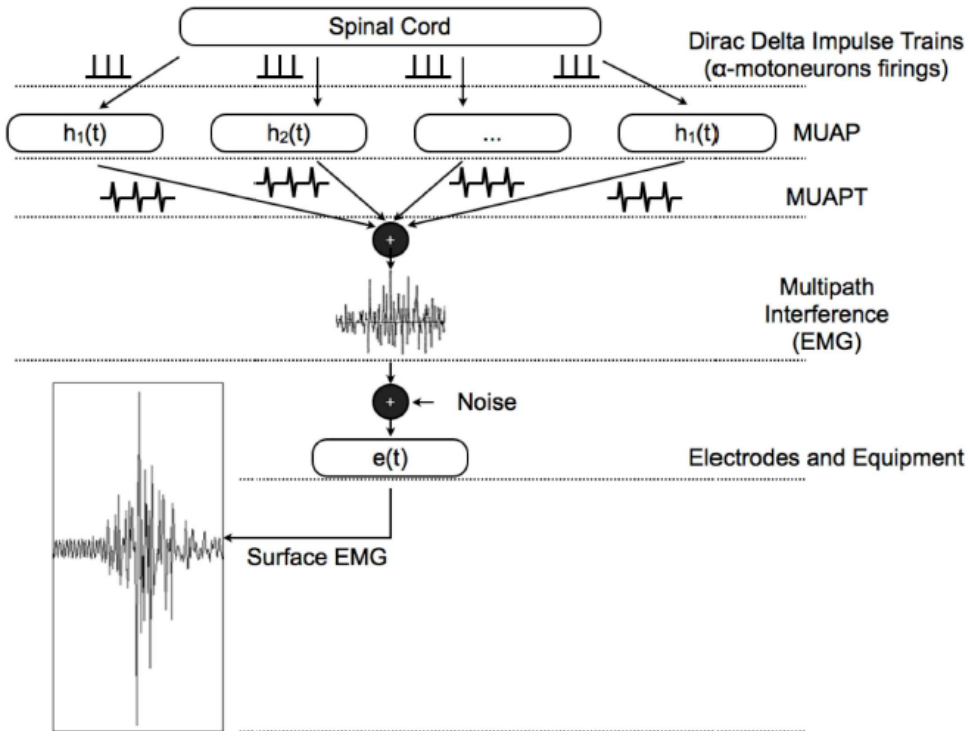


Figure 3.4: Overview of the generation of sEMG signal [17].

3.1.3 The Raw Surface EMG Signal

An unfiltered and unprocessed signal detecting the superposed MUAPs is called a raw surface EMG (sEMG) signal. Figure 3.5 shows a sample raw sEMG recording done with three static contractions of a muscle. When the muscle is relaxed, a more or less noise-free sEMG Baseline can be seen. Typically, we want the baseline to be approximately or as much as possible near zero. A good target for the baseline should around 1 to 2 microvolts and the average should not exceed higher than 3 to 5 microvolts [15].

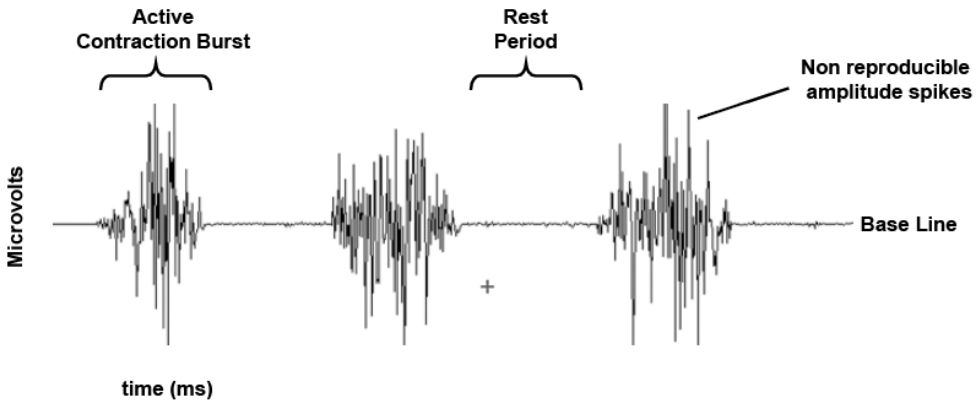


Figure 3.5: A sample raw EMG recording of 3 contraction bursts [15].

Another interesting feature of the raw sEMG signal is that these signals are stochastic in nature or that raw sEMG spikes follow random shape. This means that a raw sEMG recording cannot be reproduced in the exact shape. By applying a smoothing algorithm or selecting a proper amplitude parameter (e.g. area under the rectified curve), the non-reproducible contents of the signal is eliminated or at least minimized.

Raw sEMG signals can range between ± 5000 microvolts and typically the frequency contents ranges between 6 and 500 Hz, showing most frequency power between 20 and 150 Hz. However, in practical applications, sEMG signals are amplified and typically read in the millivolts range.

3.1.4 Factors Affecting Surface EMG Signal

Surface EMG signals are usually described as noisy signals as the EMG signal can be influenced by several external factors that can alter its shape and characteristics. The following listed below describes some these factors:

1. Tissue Characteristics - the human body is a good electrical conductor, but unfortunately the electrical conductivity varies with tissue type, thickness, physiological changes and temperature. These conditions greatly vary from subject to subject which can prohibit a direct quantitative comparison of EMG amplitude parameters calculated on the unprocessed EMG signal [15].
2. Cross Stalks - neighboring muscles (not directly in contact with the electrode) may also produce significant amount of EMG. This can contaminate the target muscle under investigation with signals from other sources.
3. Electrode and Muscle Displacement - in any movement related studies, movement of electrodes, cables and connectors are unavoidable. Any change in distance between the target muscle (signal origin) and the electrode (detection site) will alter the EMG reading. Motion artifacts can also contribute to unwanted noise in the low frequencies (less than 10 Hz).
4. External Noise - special care must be taken in noisy electrical environments. One such noise is the 50 or 60 Hz noise coming from AC power outlets which power many of the hardware and appliances. Incorrect or poor grounding of the EMG devices or other external devices may also contribute as external noise.
5. Electrode and Amplifiers - the selection of the types of electrode and amplifiers is very crucial. Internal amplifier noise should not exceed 5 Vrms. Many hardware factors can be minimized or avoided by accurately preparing and checking the given laboratory or room condition.

3.2. Detecting and Recording Surface EMG Signals

A typical electromyographic device consists of using electrodes (signal detection), an amplifier (signal amplification and modication), an analog-to-digital (A/D) converter, and a recorder (signal storage).

3.2.1 Electrodes

Electromyographic signals are detected using different types of electrode. The electrodes can usually be divided into two classes, one using invasive or needle EMG

electrodes and the other using surface electrodes. In this thesis, we focus on the use of the latter choice because of their non-invasive nature. Surface electrodes are easily handled and maintained but have the limitation of detecting only surface muscles. For deeper muscles, fine-wire or needle types of electrodes are usually preferred.

Two types of configuration are quite often used for surface EMG signals. The first is a monopolar configuration, which only uses one electrode at each target muscle and a common reference or ground electrode. Monopolar configuration has lower spatial resolution and can also can many unwanted signal from other muscles, because every electric potential between the electrode and ground are sampled. The second one is the bipolar configuration that uses two electrodes at the target muscle, which was used in this thesis. The bipolar configuration has much better spatial resolution and has a better noise reduction ability because it is the difference between two monopolar EMG signal that is amplified and read. Crosstalks and noise common to both the electrodes are removed.

For surface electrodes, Ag/AgCl pre-gelled electrodes are the most often used electrodes and recommended for the general use (SENIAM). The electrode diameter (conductive area) are typically sized from 1 cm or smaller. Commercial disposable electrodes are manufactured as wet gel electrodes or adhesive gel electrodes. Generally wet-gel electrodes have better conduction and lower impedance than adhesive gel electrodes. The latter one has the advantage that they can be repositioned in case of errors.

Factors such as electrode size and shape, inter-electrode distance, electrode positions over the target muscle can affect the detected EMG signal and hence should be held as constant as possible throughout an experiment.



Figure 3.6: Regular EMG/ECG electrodes by AMBU-Blue Sensors

3.2.2 Signal Amplification and Sampling

In the case of the bipolar electrode configuration, EMG-amplifier act as differential amplifiers which has an interesting feature to reject and eliminate artifacts. The differential amplification detects the potential differences between the two electrodes and cancels common external interference in the electrodes. EMG-amplifiers are also sometimes referred to as pre-amplifiers because they are placed in cables or directly on top of surface electrodes, where the EMG signal can be intercepted as early as possible. This placement is done to avoid amplifying motion and other artifacts. The most important amplifier characteristics are:

1. Gain - the ratio between the output voltage and the input voltage. A typical bioamplifier has gain between 100 to 10,000.
2. Input Impedance - the amplifier should have a value of at least 10x the given impedance of the electrode. It has to be high enough to avoid attenuation.
3. Common mode rejection rate (CMRR) - represents the relationship between differential and common mode gain. The CMRR should be as high as possible. A CMRR of 2000:1 expresses that all but 1/2000 of the hum will be eliminated.
4. Frequency Response - the frequency range of an EMG amplifier (bandpass settings) should start from 10 Hz highpass and go up to 500 Hz lowpass.

3.2.3 A/D Conversion and EMG Sampling Rate

Before a signal can be displayed and analyzed in the computer, it has to be converted from an analog voltage to a digital signal (A/D conversion). The resolution of A/D measurement boards have to properly convert the expected amplitude range (e.g. +/- 5 Volts). A 12 bit A/D board at the least is sufficient and can separate the voltage range of the input signal into 4095 intervals.

Nyquist theory for sampling rate states that to properly reconstruct a signal, the sampling rate needed must be twice as high as the expected frequency of the signal. For EMG signals, most of the signal power is located between 10 and 500 Hz. So a recommended sampling frequency of at least 1000 Hz is needed to avoid signal loss. Using a much lesser frequency setting can remove important information contained in the EMG can also result to anti-aliasing effects.

3.3. EMG Signal Processing

The raw EMG signal contains very important information about the corresponding target muscle innervation. However, the raw EMG signal does not explicitly give any specific meaningful analysis of the signal because of its random nature and being a mixture of noise and other external signal sources. Therefore typical analysis techniques of EMG signals that are commonly applied are by using the and analyzing features of the EMG signal such as mean, variance, root-mean-square, autocorrelation, power spectral density, and many others. However before getting these features, some established processing methods such as *rectification*, *filtering and smoothing*, and *normalization* are introduced prior to such analysis on the signal.

3.3.1 Full-wave Rectification

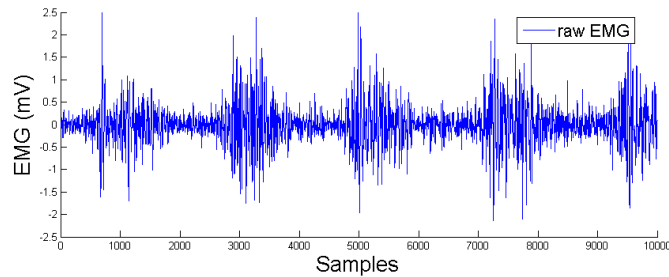
In the rectification of the EMG signal, all negative amplitudes are converted to positive values (Figure 3.7b). In this way, standard amplitude parameters such as peak or max value, area, and mean of the signal are easily obtained. In the rectified signal, the mean is a non-zero in contrast to the raw EMG signal which has a mean of zero. Rectification is done in either real-time or during post processing of the data prior to other steps such as averaging, smoothing, and etc.

3.3.2 Smoothing

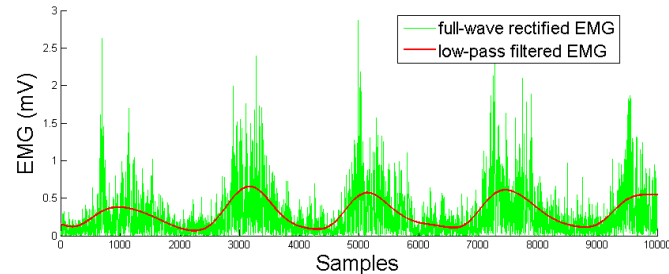
As mentioned earlier, EMG signal is stochastic in nature and cannot be reproduced the second time by its precise shape. To address this issue, the non-reproducible part of the EMG is minimized by applying digital or smoothing filters that can outline the general trend or envelope of the signal. Applying a low-pass filter, for example, is often used to create a linear envelope from a rectified EMG signal. An example of such a filter is a Butterworth low-pass filter (2nd order or higher) with cut-off frequency of 2 to 6 Hz. Using higher order digital filters can be used to minimize phase shift in the signal. Introducing phase shift in the EMG signal can intuitively be viewed as adding unwanted time delays. To solve this problem, zero-phase filters can be used to avoid any phase shifts in the signal.

Figure 3.7b shows a sample of a filtered sEMG signal using a zero-phase, second order lowpass Butterworth filter with cut-off frequency of 4 Hz.

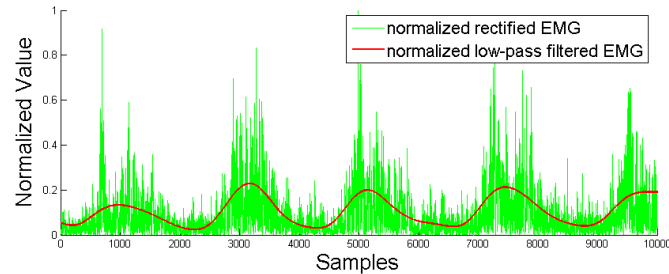
Lowpass filtered EMG signals are also quite often used to characterize EMG-Force transformations. Although the electrical signal that passes through the muscle has frequency components over 100 Hz, the force that the muscle generates is of much lower frequencies [18]. Thus, in order for the EMG signal to be correlated with the muscle force, it is important to filter out the high-frequency components.



(a) Raw sEMG recording



(b) Rectified and filtered sEMG



(c) Normalized, rectified, and filtered sEMG

Figure 3.7: Different stages of the preprocessing part of the sEMG signal.

3.3.3 Normalization

Rectified EMG signals are most often normalized by dividing the instantaneous amplitude by the value obtained while performing *maximum voluntary contraction* (MVC) of the target muscle. This is one of the most common type of normalization used and is called the MVC-normalization. Normalization is often done to reduce variability between subjects and in terms of EMG amplitudes and to have a uniform amplitude scale values between 0 to 1 as shown in Figure 3.7c. This uniform scaled value is often expressed as a percentage of the maximum voluntary contraction.

Trials to obtain the maximum voluntary contractions of the target muscles are often done prior to the test trials. MVC contractions are performed against static resistance. Though this process may sound easy to perform, but practical experiments, true MVC values are difficult to obtain. Normal untrained subjects may have problems producing a true MVC contraction level, for not being used to such efforts.

Because the reliability for getting true MVC values is very low, sometimes an *acceptable maximum effort* (AME) or the peak rectified EMG value in all trials obtained in clinical settings used for biofeedback oriented treatment can be used as a substitute for the MVC. This is particularly useful for elderly subjects and those with injuries who have may difficulty in achieving maximum effort in MVC trials. However, under estimation of the true MVC is still a potential significant source of error.

3.4. Applications of Using sEMG Signals

Surface EMG signals, in the viewpoint of engineering, has been used even as early as 1970 as an input signal for controlling signals. Saridis et. al. created a pattern recognition system using EMG signals for controlling a prosthetic arm [19]. They classified various hand movements such as elbow flexion, extension and wrist supination and pronation. This trend even became stronger in the 90's when more attention shifted back to the exploration of neural networks and the use of time-series analysis. During this time, Kiguchi et al. used fuzzy logic based neural network selection to control arm exoskeletons using EMG signals from the shoulder and upper arm region [20]. Huang et. al. also used neural network and developed a multi-degree prosthetic control, being able to discriminate 8 types of hand movement such as chucking, grasping, and flexing and extending [21].

Even up to recently, many researches on classification of hand motions using sEMG signal are extensively still being studied. With more advance machine learning techniques, more and more hand gestures are being classified with fewer but more meaningful analysis of EMG channels. More practical applications have also come to fruition controlling robots and applying to actual patients, say, patients recovering from stroke etc. For instance, Tsuji et. al. used time-recurrent based neural network for discriminating arm motion to continuously control a robot manipulator to help patients recovering from stroke and paralysis do simple desktop tasks [2].

In the field of replicating motions, discrete classification of hand gestures have been successful. Researchers investigating hand and finger classification and pattern recognition analysis have enjoyed great success, reaching a decoding accuracy of above 95% and classifying to up to more than 20 gestures [13, 22, 23, 24].

However, natural hand movements are not limited to discrete gestures but are continuous and coordinated. For rehabilitation tasks where the patient cannot move his fingers that easily it is rather important to find the position of fingers on finer levels. This research aims to predict multiple finger joint-angles simultaneously and continuously from inputs based on an EMG-to-Muscle activation model. Next chapter is devoted to continuous estimation of finger joint angles and the model used. But before we go there, commonly used EMG features which are central to the success of many previous research are going to be discussed next.

3.5. Time Domain Features of sEMG Signals

Researchers have found that there is useful information in transient burst of EMG signals than in instantaneous values of EMG signal. They have found that there is considerable structure in EMG signals during onset and that they were distinct for different types of contractions. Further works have demonstrated that transient EMG signals have greater classification capacity than steady-state signal. Because of this, different features such as time-domain features of EMG have often been used in classification problems.

Over the years, there has been great success in movement classification from myographic signals, time-domain features have been widely used. They can easily be calculated and do not require any complex transformation of the signals. These features

have been used in many clinical practice, researches and many related studies mentioned earlier [13, 22, 23, 24, 18, 6].

For the purpose of comparing the joint angle estimation performance when different types of inputs are used (that of ours and of the related studies) later on, we list some of these features. Following traditional delay consideration, a sliding window was applied on the filtered sEMG signal, we used and obtained the following time-domain features:

- Mean of the Absolute Value (MAV):

$$MAV = \frac{1}{N} \sum_{i=1}^N |x_i| \quad (3.1)$$

- Waveform Length (WL):

$$WL = \sum_{i=1}^N |x_i - x_{i-1}| \quad (3.2)$$

- Willison Amplitude (WA):

$$WA = \sum_{i=1}^N f(|x_i - x_{i-1}|) \quad (3.3)$$

where $f(x)$ is 1 if $x > \text{threshold}$, or 0 if otherwise.

- Variance (VAR):

$$VAR = \frac{1}{N-1} \sum_{i=1}^N (x(i)^2) \quad (3.4)$$

These features provide different information such as those pertaining to signal amplitude, frequency, extent of muscle contraction, and extent of the firing of motor unit action potentials. These are but a handful few of the many EMG features that have been used over the years. Other important features which include the zero-crossings, Auto-regressive (AR) models of EMG, wavelets, frequency, and Cepstral-based features are also used in several applications. However the discussion and usage of other features is beyond the scope of this thesis. A more detailed information about these features are discussed in Zecca's work [13].

Chapter 4

Continuous Estimation of Finger Joint Angle from Surface EMG

Despite the success of discrete classification of more than 20 hand gestures, natural hand movement is continuous and offers an infinite number of fine hand movement variations. Studies for continuous prediction of fine finger movements has been comparatively few and less focus has been given. In this chapter we discuss some inherent problems involved in such continuous estimation of motion from EMG signals such as electromechanical delays. Though time-domain features have been used and been successful tremendously in classification of hand gestures, they may not entirely give optimal prediction performance in the case of continuous prediction. So in this chapter, we also discuss an EMG-to-Muscle activation model that may be give more useful and suitable input features.

Also, many algorithms and methods for classification have been given and discussed by related studies. Some of these include linear discriminant analysis (LDA), neural networks, and support vector machines. However for continuous prediction, regression analysis are better suited. Here in this thesis, we have used and compared both an artificial neural network (ANN), which is a famous universal approximator of any function, and a nonparametric Bayesian approach method in the form of a Gaussian Process (GP). This chapter also provides the necessary theories and a short background behind the neural network and Gaussian Process regressors.

4.1. Problems of Electromechanical Delay

For any intended motor action, it is known that there occurs a time delay, which is known as the *electromechanical delay* (EMD), between the onset of the sEMG signals and the exerted mechanical output such as force and tension produced in the movement. EMD is also termed motor time or motor execution time in researches related to fractionated reaction time [25].

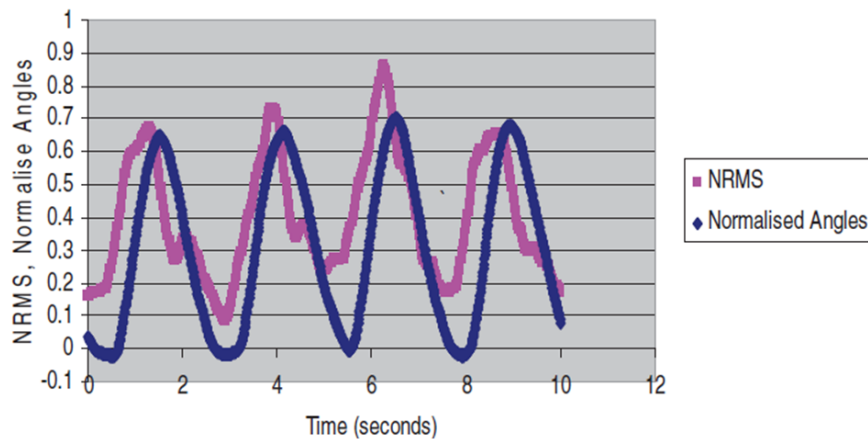


Figure 4.1: The electromechanical delay is shown as the time difference between the normalized recorded angle and root-mean-square windowed EMG.

EMD has been presented and observed by previous studies in EMG related studies involving the leg and as well as in the arm [6, 18]. A sample is shown in Figure 4.1. The normalized filtered sEMG signal (pink) leads the recorded joint angle (blue), as sEMG occurs first before force production of the task. EMD has been reported to range from 10 ms to about 150 ms, but varies differently depending on the muscle fiber type, muscle length, fatigue, training, and speed of the intended task [26].

EMD presents a challenging problem that must be resolved if valid and meaningful relationships between EMG and force, moment, or movement patterns are to be established [26]. Studies have shown that EMD varies differently and changes with certain pathology. Relatively short EMD has been observed in patients with cerebral palsy, while prolonged EMD were seen in *anterior cruciate ligaments* or more commonly known as ACL reconstructions [25]. However for cases under normal conditions, or in studies with healthy subjects, constant EMD values has often been used to tempo-

rally align EMG and force or movement related time profiles during recorded dynamic activities.

Vint et. al. concluded in their study that EMD approached a relatively constant value regardless of initial tension levels and rate of force requirements [26]. They suggested that the temporal alignment of the EMG and force or kinetic data is mainly influenced by the state of pretension and the rate of force development. They suggests that incorporating a constant temporal offset to align EMG and kinetic data may be reasonable if the actions of interest are performed from nonresting conditions or if the rate of force development is relatively fast. The value of the assumed EMD should be determined in a manner that seeks to replicate the conditions under which the kinetic data will be collected.

Thus, EMD cannot be ignored in sEMG studies involving motor actions, and must be considered accordingly.

4.2. EMG-to-Muscle Activation Model

To learn a suitable filtered signal that automatically considers EMD, we introduce the use of a so called EMG-to-Muscle Activation model. EMG is a measure of electrical activity that spreads across muscles, which causes the muscles to activate. This results to the production of force, to which the model used transforms the sEMG signals to a suitable force representation. A raw EMG signal is a voltage that is both positive and negative, whereas muscle activation is expressed as a number between 0 and 1, which is smoothed or filtered to account for the way EMG is related to force [18].

Zajac modeled this muscle activation dynamics using a first-order recursive filter [27]. Although a first-order differential equation does a fine job of characterizing activation, Buchanan et. al. created a second-order model filter that works efficiently to model the relationship between EMG and muscle activation [18]. Because the muscle fiber is activated by a single action potential, the muscles generate a twitch response and this type of response is well represented by a critically damped linear second-order differential system to determine neural activation $u(t)$:

$$u(t) = M \frac{de^2(t)}{dt^2} + B \frac{de(t)}{dt} + Ke(t) \quad (4.1)$$

where M , B , and K are constants that define the dynamics of the second-order system.

Because in the lab setting, the data are sampled at discrete time intervals, we make use of their filter in its approximate discrete version given by:

$$u_j(t) = \alpha e_j(t-d) - \beta_1 u_j(t-1) - \beta_2 u_j(t-2) \quad (4.2)$$

where $u_j(t)$ is the so-called neural activation, and $e_j(t)$ is the normalized, rectified and filtered EMG of muscle j at time t . In this model, α , β_1 , β_2 are recursive coefficients of the filter and d is the EMD. Filter stability is guaranteed by putting constraint conditions on α , β_1 , and β_2 .

$$\beta_1 = \gamma_1 + \gamma_2 \quad (4.3)$$

$$\beta_2 = \gamma_1 \cdot \gamma_2 \quad (4.4)$$

$$|\gamma_1| < 1, |\gamma_2| < 1 \quad (4.5)$$

$$\alpha - \beta_1 - \beta_2 = 1 \quad (4.6)$$

In the filter model, neural activation depends not just on the current level of EMG, but also on its recent history, or the last values of $u_j(t)$. Here, the value for the neural activation is constrained from 0 to 1.

Also because studies have also shown that while some muscles have linear isometric EMG-to-force relationship, the relationship for other muscles is nonlinear. To model this nonlinearity between neural activation and muscle activation, the transformation to the muscle activation v_j is then given by:

$$v_j = \frac{e^{A_j u_j(t)} - 1}{e^{A_j} - 1} \quad (4.7)$$

where A_j is a parameter that introduces the nonlinearity between EMG and muscle activation, and is constrained between -3 and 0 , with -3 being highly exponential and 0 being linear. The effect that the parameter A_j has on the muscle activation in terms of the neural activation is described by Figure 4.2.

Using the model discussed, the pre-processed EMG is transformed to its muscle activation dynamics, the converted signal is now suitable and can be used as a continuous input to a regressor. The transformation from the raw EMG to its pre-processed filtered form then to its muscle activation is seen in Figure 4.3.

The EMG-to-Muscle Activation model not only solves the EMD of the muscle, but also requires only a few parameters. The parameters of this filter, γ_1 , γ_2 , d , and

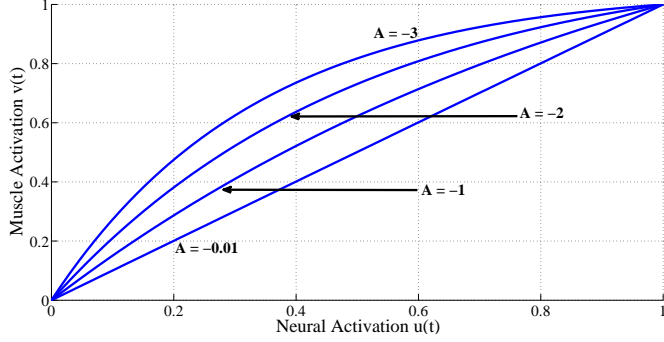


Figure 4.2: The parameter A introduces nonlinearity between the neural activation and muscle activation.

A are obtained by using constrained nonlinear programming in Matlab's Optimization Toolbox to minimize a mean-square error cost function:

$$\frac{1}{N} \sum_t (\theta_{est} - \theta_{target})^2 \quad (4.8)$$

where N is the total number of samples, and θ_{est} and θ_{target} are the predicted and measured finger joint angles, respectively. Aside from the constraints given in equations 4.3 to 4.6, the time delay parameter d is also constrained within its physiological limits, which is between 10 and 150 ms.

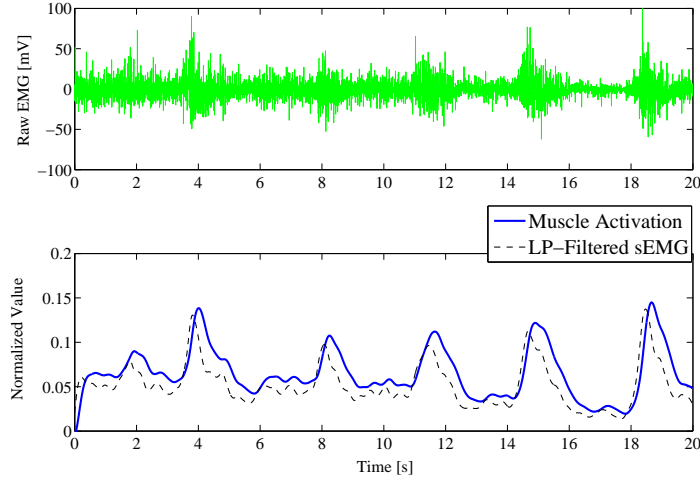


Figure 4.3: A sample raw EMG recording is low-pass filtered and converted to its muscle activation form.

If we only want to map the EMG signals to a single finger's joint angles and if the training time needs to be really fast, then a linear estimation of the joint angles to obtain θ_{est} would suffice. However, there is no clear defined model or clear relationship that yet exist between the muscle activation and the produced finger joint angles. The relationship between these two are often assumed to be nonlinear. Hence, in this thesis, we resort to using an artificial neural network and a Gaussian Process as our nonlinear estimator.

4.3. Regression Methods

4.3.1 Artificial Neural Network

In general, neural networks are considered to be attractive for nonlinear modelling because of their ability to approximate any arbitrary functions [28]. Because of this, we predicted all 15 joint angles of the fingers simultaneously and continuously using an artificial neural network (NN):

$$\theta_{est}(t) = NN(\mathbf{v}(t), \mathbf{w}) \quad (4.9)$$

where $\theta_{est}(t) \in \mathbf{R}^{15 \times 1}$ is the predicted finger joint angle, $\mathbf{v}(t) \in \mathbf{R}^{8 \times 1}$ is the muscle activation input, and \mathbf{w} are the weight parameters which represent the links between the nodes or neurons.

In our study, a multilayer feed forward network was used. The network is made up of an input layer, a hidden layer(s), and a single linear output layer (see Figure 4.4). Generally, the use of this type of artificial neural networks belongs to a class in machine learning called *supervised learning*. It is called in such a way because the training phase of the learning is carried out in a way that the ANN regressor has to learn how to associate each training input vector sample to an associated label called a *target output*.

An artificial neural network consists of a topological graph of neurons, with each neuron computing the activation function of the inputs and sends the result in the output layer. Suppose a set of input features is denoted by \mathbf{x} , then the first step to feedforward neural network is to transform the inputs corresponding to the weights and shift by a

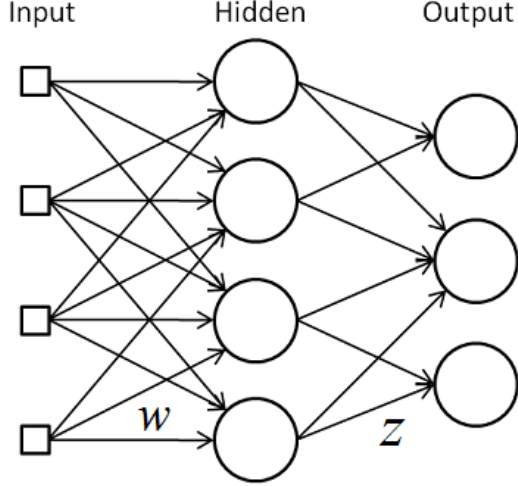


Figure 4.4: The architecture of a multilayer feedforward artificial neural network.

bias factor specific to each neuron given by a_j :

$$a_j = \sum_{i=1}^D w_{ji}^{(1)} x_i + w_{j0}^{(1)} \quad (4.10)$$

where the w_{ji} are the given weights of each neuron. Here we assume that we have a dataset D of n observations, denoted by $D = \{(x_i, y_i) \mid i = 1, \dots, n\}$. Then a_j is transformed using a select activation function such as *sigmoid* or *tan-sigmoid* activation function. In this thesis, a tan-sigmoid activation function given by z_j was used.

$$z_j = h(a_j) = \frac{e^{a_j} - e^{-a_j}}{e^{a_j} + e^{-a_j}} \quad (4.11)$$

Then the elements of the output (or target) vector \mathbf{y} is computed as:

$$a_k = \sum_{i=1}^M w_{kj}^{(2)} z_j + w_{k0}^{(2)} \quad (4.12)$$

$$y_k = a_k \quad (4.13)$$

It has been shown that for certain neural network topologies, with the right set of weights and biases, any continuous function can be accurately approximated [28].

The use of an ANN has two phases; a training phase and a test phase. During the training phase, the ANN is trained to return a specific output given a specific input. Training is done by presenting the ANN a set of training data and adjusting the

parameters between each layer. The learning problem consists of finding the optimal combination of weights w_{ji} so that the network output approximates a given target output as closely as possible. To achieve this, the training algorithm tries to minimize a mean-square error between the target t and predicted output y values given by:

$$E = \frac{1}{N} \sum_i (y_i - t_i)^2 \quad (4.14)$$

In the test phase, the ANN returns the output based on the propagation of the input through all the layers.

In the scope of the thesis, the input layer had 8 nodes coming from the muscle activation of the each muscle, while the output has 15 nodes consisting of the finger joint angles. To train the network, we input a set of training data to the neural network and minimize a mean square error function. The most common way to minimize the error is through the use of a *backpropagation* algorithm. But since another method, such as the Levenberg Marquardt (LM) algorithm, appears to be the fastest method for training moderate-sized feedforward neural networks. In this thesis, we used the LM algorithm.

We evaluated the network's performance with various number of neurons in the hidden layer, ranging from 5 to 250. Using a fixed training set, we chose the specific number of neurons in the hidden layer based on which solution gave the smallest average error on an unseen test set. Also to avoid overfitting, total data set was divided into a training and a validation set and apply an early stopping method during training iterations [29].

4.3.2 Gaussian Process for Regression

In this study, we also evaluated the finger joint angle estimator performance when another general nonlinear estimator was used. In this thesis, we used a nonparametric Gaussian Process (GP) regressor shown in equation below:

$$\mathbf{y} = \text{GP}(m(\mathbf{x}), k(\mathbf{x}, \mathbf{x}')) \quad (4.15)$$

where \mathbf{x} is the input, \mathbf{y} is the estimated or predicted output coming from the dataset denoted by $D = \{(x_i, y_i) \mid i = 1, \dots, n\}$ and the Gaussian process is determined by a mean function $m(\mathbf{x})$ and covariance function $k(\mathbf{x}, \mathbf{x}')$. Relating this to the thesis's goal

of predicting finger joint angles from EMG signal, we can substitute \mathbf{x} with \mathbf{v} which is the muscle activation input. And the target \mathbf{y} with the joint angle estimate θ_{est} .

The main reason why we introduced the use of another regressor, in the form of a more popular nonparametric Bayesian approach using Gaussian Process, is that we wanted to see if the prediction of the finger joint angles, PIP and DIP finger joint angles, from EMG signals can be greatly improved.

Gaussian processes regression is fundamentally different from feed-forward networks. Rather than capturing regularities in the training data via updating neuron weights, it applies a Bayesian inference to explicitly compute a posterior distribution over possible output values y given all the data and the new input x [30, 31].

Formally, a Gaussian process generates data located throughout some domain such that any finite subset of the range follows a multivariate Gaussian distribution [32]. From an n observations in an arbitrary dataset, $\mathbf{y} = y_1, \dots, y_n$, can always be imagined as a single point sampled from some multivariate Gaussian distribution. Hence, such a data can be partnered with a GP.

Very often, it is assumed that the mean of this partner GP is zero everywhere:

$$m(\mathbf{x}) = 0 \quad (4.16)$$

What relates one observation to another in such cases is just the covariance function $k(\mathbf{x}, \mathbf{x}')$. A popular choice is a *Gaussian* or a *squared exponential* covariance function given by:

$$k(\mathbf{x}, \mathbf{x}') = \sigma_f^2 \exp \left[\frac{-(\mathbf{x} - \mathbf{x}')^2}{2l^2} \right] \quad (4.17)$$

where the maximum allowable covariance is defined as σ_f^2 . Here, σ_f and l are called *hyperparameters*. If $\mathbf{x} \approx \mathbf{x}'$, then $k(\mathbf{x}, \mathbf{x}')$ approaches the maximum covariance value, meaning the underlying function $f(\mathbf{x})$ is nearly perfectly correlated with $f(\mathbf{x}')$. Now if \mathbf{x} is distant from \mathbf{x}' , then $k(\mathbf{x}, \mathbf{x}') \approx 0$. So, for example, during interpolation at new x values, distant observations will have negligible effect. The hyperparameter l controls the effect of the separation between $f(\mathbf{x})$ and $f(\mathbf{x}')$.

Data are often treated with the consideration of noise. So each observation y can be thought of as related to an underlying function $f(x)$ through a Gaussian noise model:

$$y = f(\mathbf{x}) + N(0, \sigma_n^2) \quad (4.18)$$

Generally, the problem defined for a regression is the search for the underlying function $f(x)$ that can best model the data D . To consider the noise into the covariance function, we can rewrite $k(\mathbf{x}, \mathbf{x}')$ as:

$$k(\mathbf{x}, \mathbf{x}') = \sigma_f^2 \exp\left[\frac{-(\mathbf{x} - \mathbf{x}')^2}{2l^2}\right] + \sigma_n^2 \delta(\mathbf{x}, \mathbf{x}') \quad (4.19)$$

where $\delta(\mathbf{x}, \mathbf{x}')$ is the *Kronecker Delta Function*. So given n observations of y , the objective is to predict y_* and not the actual f_* , whose expected values are identical but with different variance due to the observational noise. To prepare the GP regression, the covariance function among all the possible points are calculated which we denote as the following:

$$K = \begin{bmatrix} k(x_1, x_1) & k(x_1, x_2) & \cdots & k(x_1, x_n) \\ k(x_2, x_1) & k(x_2, x_2) & \cdots & k(x_2, x_n) \\ \vdots & \vdots & \ddots & \vdots \\ k(x_n, x_1) & k(x_n, x_2) & \cdots & k(x_n, x_n) \end{bmatrix} \quad (4.20)$$

$$K_* = \begin{bmatrix} k(x_*, x_1) & k(x_*, x_2) & \cdots & k(x_*, x_n) \end{bmatrix} \quad (4.21)$$

$$K_{**} = k(x_*, x_*) \quad (4.22)$$

In GP modelling, the key assumption is that the data can be represented as a sample from a multivariate Gaussian distribution,

$$\begin{bmatrix} \mathbf{y} \\ y_* \end{bmatrix} \sim \mathcal{N}(0, \begin{bmatrix} K & K_*^\top \\ K_* & K_{**} \end{bmatrix}) \quad (4.23)$$

To predict y_* , we are interested in the conditional probability $p(y_* | \mathbf{y})$, which means that given the training data y , how likely is a certain prediction for y_* is. As explained more in [31, 32], the probability follows a Gaussian distribution:

$$y_* | \mathbf{y} \sim \mathcal{N}(K_* K^{-1} \mathbf{y}, K_{**} - K_* K^{-1} K_*^\top) \quad (4.24)$$

The predictive value for y_* is the mean of the probability distribution:

$$\bar{y}_* = K_* K^{-1} \mathbf{y} \quad (4.25)$$

and the uncertainty in the estimate is capture by its variance:

$$\text{var}(y_*) = K_{**} - K_* K^{-1} K_*^\top \quad (4.26)$$

The reliability of the GP regression is highly dependent on the chosen covariance function. A maximum posterior estimate of the hyperparameters \mathbf{w} (e.g. $\mathbf{w} = \{\sigma_f, \sigma_n, l\}$) occurs when the posterior probability $p(\mathbf{w} | \mathbf{x}, \mathbf{y})$ is at its greatest. Baye's theorem tells us that, assuming there is little prior knowledge about what \mathbf{w} should be, this corresponds to minimizing the negative log likelihood given by:

$$\ln p(\mathbf{y} | \mathbf{x}, \mathbf{w}) = -\frac{1}{2}\mathbf{y}^\top K^{-1}\mathbf{y} - \frac{1}{2}\ln|K| - \frac{n}{2}\ln 2\pi \quad (4.27)$$

Running a multivariate optimization algorithm (e.g. conjugate gradients), or by using an *exact inference* method, good choices for \mathbf{w} can be obtained [31].

In this thesis, GP regression was implemented using the Gaussian Process Regression and Classification Toolbox [33]. The EMG data was re-normalized and standardized to have the mean value of each feature equal to 0 and the standard deviation equal to 1. The input feature that we used was the 8-dimensional muscle activation feature vector as discussed previously in Section 4.2. The GP configuration used an assumed mean function of 0. The likelihood function was assumed to be Gaussian (with one hyperparameter σ_n), and the covariance function to be a squared exponential function, which takes two additional hyperparameters (a characteristic length-scale, l and unit signal standard deviation, σ_f) [31]. An exact inference method was used, and we optimize over the hyperparameters by minimizing the negative log marginal likelihood w.r.t. to the hyperparameters.

However in this method, each of the joint angles were independently predicted from the muscle activation inputs. Unlike in the use of the artificial neural network where one network produced all 15 joint angle outputs simultaneously, in the GP regression, a separate GP model was made for each finger. In the training stage, 15 GP regressors were trained from the same set of training input.

Chapter 5

Experiments

To validate the use of the chosen EMG features and the regression model, experiments involving the record of sEMG signals and hand and finger movements were conducted. This chapter explains the experimental set-up and the process, tasks, and conditions that the subjects underwent.

5.1. Experimental Set-up

The system is composed of a wireless surface electromyograph and an optical motion capture device. Surface EMG signals were extracted from eight extrinsic muscles of the hand that are known to contribute to wrist and finger movements. These target muscles along with their corresponding function related to any hand or finger movements are listed in Table 5.1.

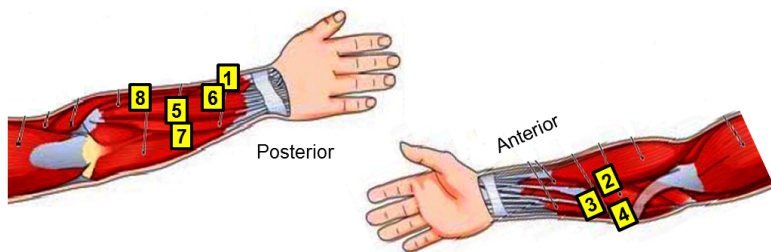


Figure 5.1: Electrode placement was based on muscle locations related to hand and finger movements.

Table 5.1: Selected EMG channels and the target muscles.

Ch	Target Muscle	Hand/Finger
1	Abductor pollicis longus	Thumb abduction
2	Flexor carpi radialis	Wrist, hand flexion and abduction
3	Flexor digitorum superficialis	2-5th finger PIP flexion
4	Flexor digitorum profundus	2-5th finger DIP flexion
5	Extensor digitorium	2-5th finger extension
6	Extensor indices	Index finger
7	Extensor carpi ulnaris	Wrist extension and abduction
8	Extensor carpi radialis	Wrist and thumb

Eight bipolar active-type Ag/AgCl electrodes from AMBU (see Figure 3.6), with inter-electrode distance of 20 mm were placed on the subjects dominant forearm as shown in Figure 5.1. A single electrode was also placed on the subjects olecranon to serve as ground and reference electrode.

The sEMG device that was used was a BA1104 amplifier with a telemetry unit TU-4. The hardware provided a high-pass filter with cut-off frequency of 1 kHz during the EMG data acquisition process. The set-up configuration for this amplifier and telemeter unit is shown in Figure 5.2. All sEMG device components came from Digitex laboratory co. ltd..

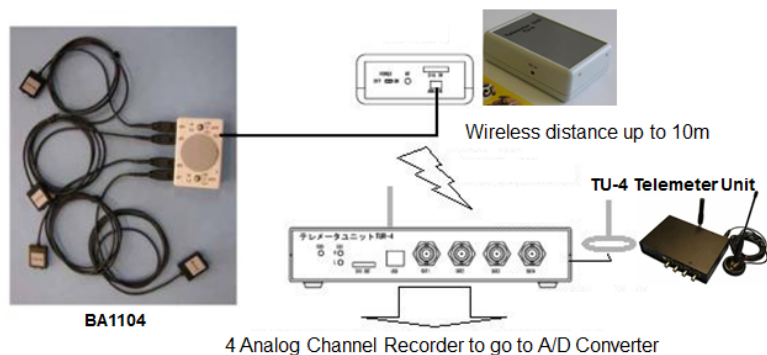


Figure 5.2: The wireless sEMG device is based on a BA1104 biological amplifier and a wireless telemeter unit from Digitex Laboratory.

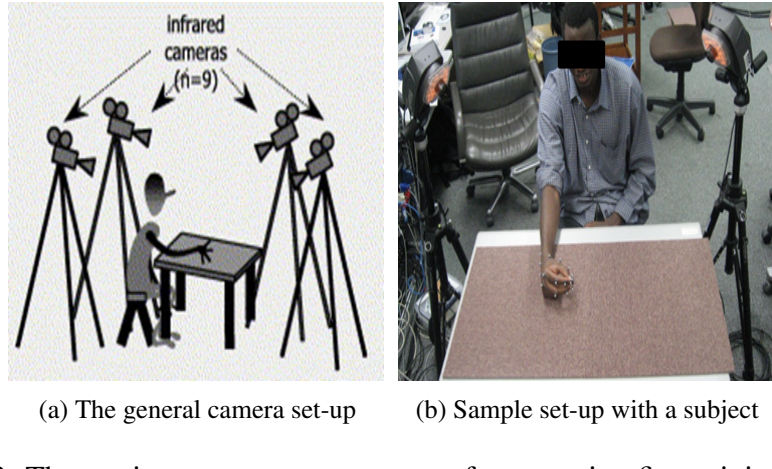


Figure 5.3: The motion camera system set-up for capturing finger joint positions.

While finger movements were made, the hand and finger motion were recorded simultaneously using a MAC3D motion capture system (Motion Analysis Corp.). The camera set-up is shown in Figure 5.3. Twenty-two passive reflective markers for motion capture were also attached on the subject's hand, with each marker located on each joint of the finger and as well as three in the wrist area (see Figure 5.4). The software that we used for both the motion and sEMG signal capture were the Evart and Cortex software from Motion Analysis. A sample screenshot of the data acquisition is shown in Figure 5.5.

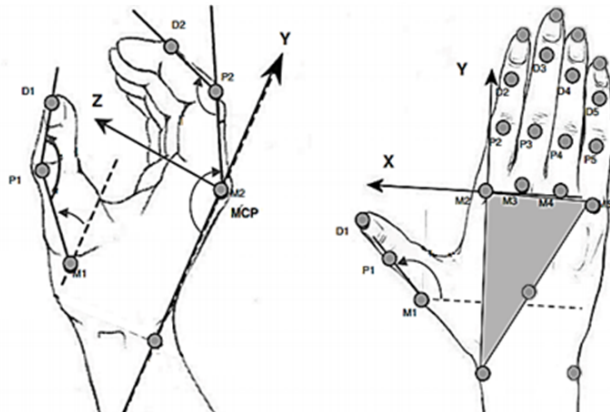


Figure 5.4: Twenty-two reflective markers are attached on the joints of the hand.

The sEMG signals were sampled at 2 kHz, and were inputted to the A/D converter. The finger motions were sampled at 200 Hz with measurement units in millimeter, having a precision of 0.5 mm but relatively changes each time the cameras are calibrated. With the x, y, z positions of each marker continuously recorded, the joint positions, namely the MCP, PIP, and DIP joint angles were also calculated.

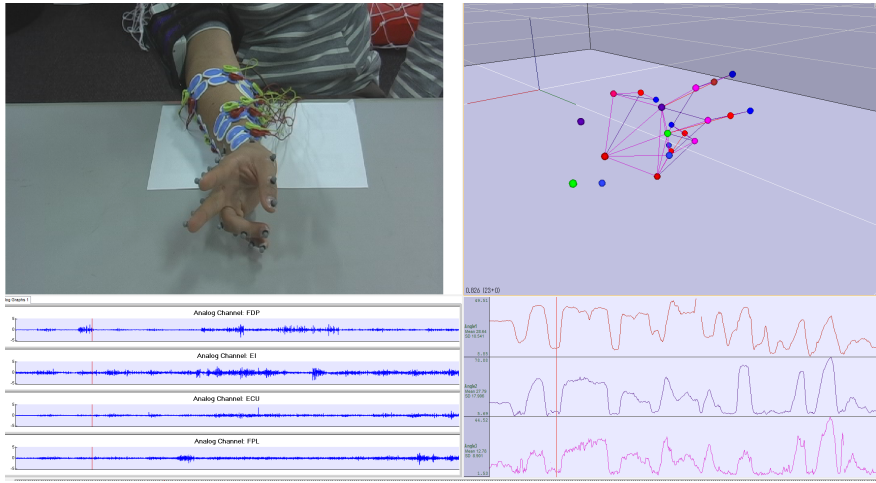


Figure 5.5: A screen capture showing the subject's hand and the corresponding hand model while the sEMG and the motion data were simultaneously recorded.

5.2. Data Collection

Two volunteer healthy subjects (male, mean age of 25, right-handed), with no known physical impairments, were seated with their elbow positioned on a flat surface in a comfortable position. Each subject was asked to do 3 different tasks. For the first part of the experiment, the subject was tasked to move one finger at a time, in the flexion and extension plane of each finger. The second task involved the subject doing flexion and extension of all fingers simultaneously. Finally for the third and last part of the experiment, the subject was asked to move any of his fingers freely and in anyway he wants. Irregular movements were encouraged from the subject in this last part of the experiment.

The first task consisted of 5 sets of movements, one for each individual finger. While the second task consisted of 2 sets and the last task consisted of 1. Overall, the

whole experiment consisted of making a total of 8 sets of movement tasks. In each set, there were 5 trials, with each trial lasting 20 seconds. All trials were sequentially done and the subject was allowed to rest anytime during the experiment. The subjects were also instructed to, as much as possible, maintain the position of the whole arm in a neutral and relaxed position while the fingers were moving.

After collecting the EMG data along with the motion capture of the finger movements, separate trials were also done to obtain the maximum voluntary contractions (MVC) of each muscle. The subjects were also asked to flex their hands and fingers in all possible plane of movements to try and induce maximum contractions for all the targeted muscles in the forearm.

Eighty percent of all the recorded data were used in training the regressor and the remaining twenty percent were used for test and validation purposes. All the data in each task were concatenated together to form a larger training and test dataset. However, the data were separated and were analyzed separately for each subject.

5.3. Data Preprocessing

The raw sEMG signals were first preprocessed into a form, that after further manipulation, can be used to predict muscle activation [18]. The sEMG signals are rectified and normalized by the maximum voluntary contraction (MVC), obtained separately from each subject as explained earlier. However, it is very hard to obtain true MVC reading, so to ensure that normalization is done properly through all the muscles, we use the maximum rectified EMG values across not only from the MVC trial but throughout the entire dataset in the duration of the whole experiment.

The signals were then filtered using a 2nd-order low-pass filter with cut-off frequency of 4 Hz similar to that shown in Figure 3.7b. This is done prior to obtaining the muscle activations, which are highly related to muscle force found in low frequencies. The filtered sEMG signals were then downsampled to 200 Hz to match that of the motion data.

All the fingers produced all three joint angles of interest. The tasks were constrained to moving the fingers only in the flexion and extension plane, thus, a total of only 15 joint angles were significant. The joint angles were both computed from the marker positions (see Figure 5.4) and were also checked and recorded using the motion

analysis tools inside the Evart and Cortex software. A low-pass filter with cut-off frequency of 10 Hz was also applied on the motion data, to remove any noise and jitters in the signal.

The range of motion given by each 15 of the joint angles are given in the table below. These were based from minimum value and maximum value of the recorded joint angle data. However, to standardize and scale all the joint angle values in showing the plots and graphs in the next chapter, we normalize each finger to show a scaled value from 0 to 1. Normalization of each joint angle data was done by subtracting the minimum of the joint angle to each sample and dividing it by the norm value.

Table 5.2: Finger joints normal range of motion.

Finger Joint	Type of Motion	Theoretical Range	Measured Range
Thumb CMC	Hyperextension/Flexion	0/55 deg	0/32 deg
Thumb MCP	Hyperextension/Flexion	-10/55 deg	0/58 deg
Thumb IP	Hyperextension/Flexion	-15/80 deg	-5/70 deg
Finger MCP	Extension/Flexion	-45/90 deg	-30/74 deg
Finger PIP	Extension/Flexion	0/100 deg	0/80 deg
Finger DIP	Extension/Flexion	0/80 deg	0/35 deg

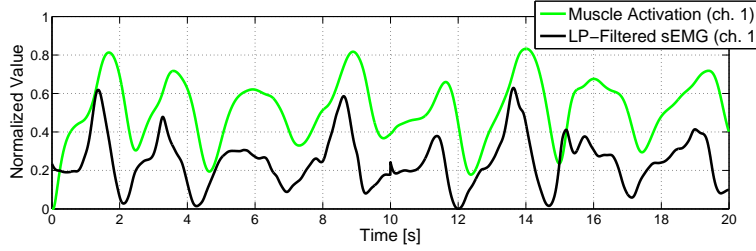
Chapter 6

Results and Analysis

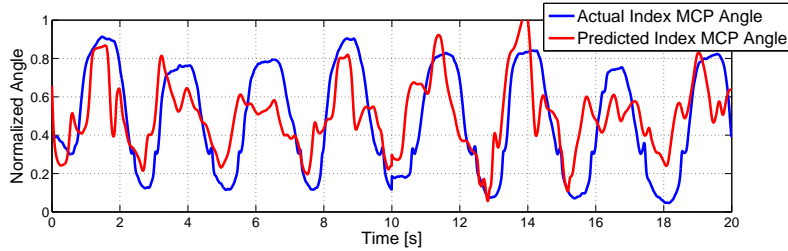
This chapter presents results obtained in predicting finger joint angles from sEMG using the proposed EMG-to-muscle activation features. The proposed method is compared with using conventional time-domain features, commonly used by previous related studies. Performance of the ANN-based and GP-based regressors are also shown and some trade-offs in using one from the other are discussed. Moreover, a dimensionality analysis of hand movements which include basic statistic analysis of hand movements are also done to help us draw conclusions on why predicting 15 finger joint angles were possible with the use of only a few EMG inputs.

6.1. Prediction of Finger Joint Angles from Muscle Activation Inputs

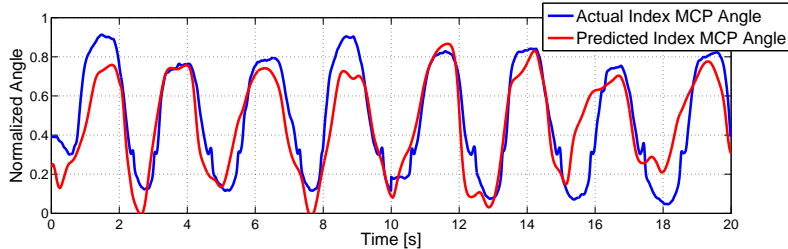
The main motivation in using an EMG-to-Muscle Activation model as input features in predicting continuous finger joint angles as discussed in Chapter 4 was that it considered electromechanical delay (EMD) as a parameter. In that method, the size of the time-scale windowing or segmenting of EMG was not an issue unlike in the use of time-domain features.



(a) Processed EMG Input Signal from Ch. 1



(b) Predicted from Filtered sEMG Input (Without EMD)



(c) Predicted from Muscle Activation Input(With EMD)

Figure 6.1: Single joint angle prediction results using muscle activation inputs that considers with and without EMD.

In Figure 6.1b and Figure 6.1c, the plots show two prediction results of a single index finger joint angle movement in a periodic flexion and extension task, one using low-pass filtered EMG, and the other using Muscle Activation inputs. Here, the predictor was an ANN trained from processed inputs shown in Figure 6.1a. Using the proposed EMG-to-Muscle Activation model is not only biologically plausible but it also determined an optimal estimate of the EMD, and requires only a few parameters for the input features. By considering EMD, we can see in Figure 6.1a that this shifts the muscle activation signal almost suitably aligning with the motion data.

Table 6.1: Muscle Activation Model Parameters

Parameter	Values Obtained
d	0.04
γ_1	-0.9748
γ_2	-0.9748
A_j	-1.26

In the training setting, the obtained parameters using the muscle activation model are shown in Table 6.1. With the neural network trained, we predicted all finger joint angles simultaneously. Figure 6.2 shows the result of the index finger joint angles in one test trial from task 1 showing a single finger flexion and extension motion.

A correlation as high as 0.92 was obtained for the MCP angle estimation, while the estimation of the PIP and DIP joint angles were consistent, which were about 0.8 and 0.7 in correlation, respectively. Processing the sEMG into its muscle activation

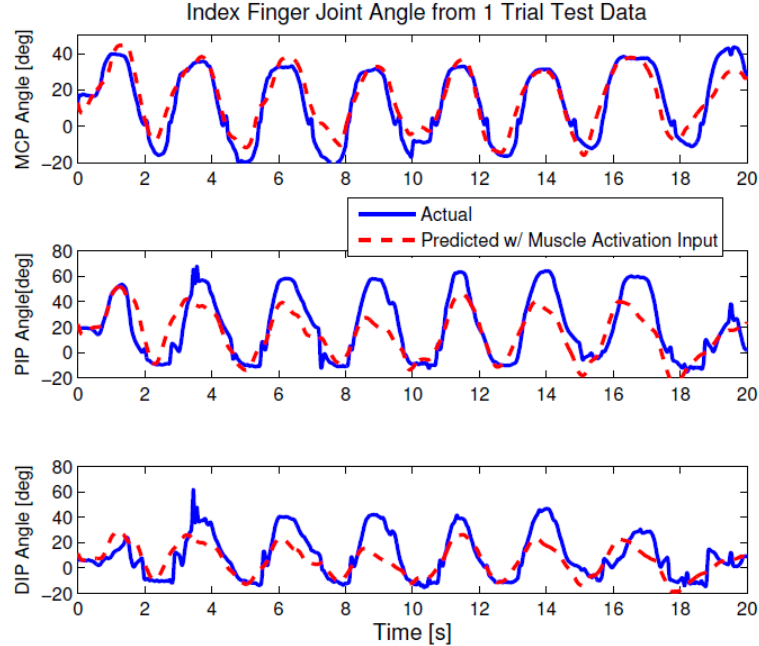


Figure 6.2: Index finger joint angle estimation for 1 test trial involving the index finger flexion and extension.

dynamics was straightforward. For this trial, the EMD obtained was 40 ms, suitably aligning the sEMG onset to the motion data. This model works very well for motion with constant velocity where EMD is approximately the same in a trial.

Similarly, Figure 6.3 shows the results of the predicted index finger joint angles involving free and random movement of the fingers. The regressor is able to predict the index finger joint angles rather well, but not as accurate as when only moving fingers one at a time. In this trial, we assume that EMD varied differently. The optimization step chooses the best possible values for EMD from the training data, but does not account for the EMD changes resulting from different velocities. Also in the previous task with the periodic motion, the two lesser angles followed movements similar to the MCP angles, but for random motions, it may totally differ. The muscle activation inputs that we use do not give an explicit feature that relates the angles to one another.

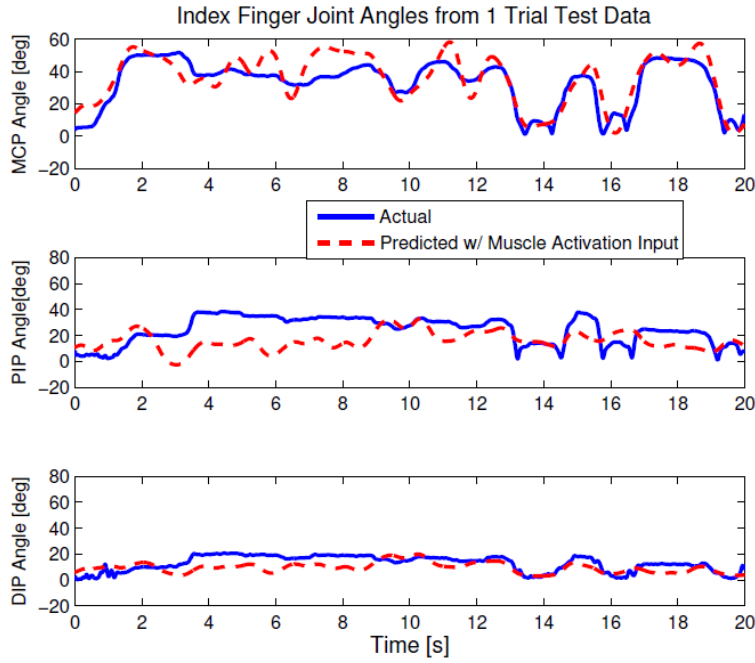


Figure 6.3: Index finger joint angle estimation for one test trial involving task 3, where the subject could move freely in anyway. The correlation coefficient between the predicted and measured MCP, PIP, and DIP angles are 0.88, 0.52, and 0.60, respectively.

6.2. Comparison Between Different EMG Features

We also want to show that using muscle activation input not only parameterizes and considers EMD, but it also gives better estimation result. Here, we compared the estimation performance of three types of input: filtered sEMG signal, sEMG time-domain features, and the proposed muscle activation model input.

The filtered sEMG signals that we used were the preprocessed sEMG signal $e_j(t)$ in equation 4.2 before any transformation was applied. The sEMG time-domain features that we used were the ones discussed earlier in Section 3.5, which are the MAV, WL, WA, and VAR of each sEMG channel.

Figure 6.4 and Figure 6.5 show the mean correlation coefficients and mean overall normalized root-mean-square error (NRMSE) of the predicted and measured finger joint angles, respectively, of all the test data. We compared the estimation performance of different inputs used by the related studies and that used by our study, which uses the muscle activation input features. The results in both figures were obtained from a 5-fold cross validation to see the overall statistical performance of the estimator.

We can see that using the proposed model gave better estimation results, higher

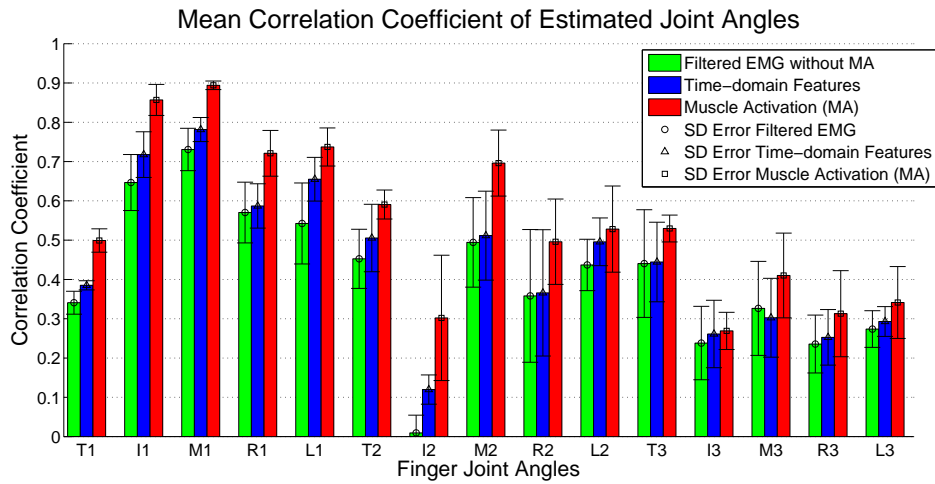


Figure 6.4: The mean correlation coefficient of the predicted and measured finger joint angles, across three different inputs: filtered sEMG, time-domain, and muscle activation inputs. The x-axis letter labels represent the thumb, index, middle, ring, and little finger, while the numbers 1,2, and 3 are the MCP, PIP, and DIP angles, respectively.

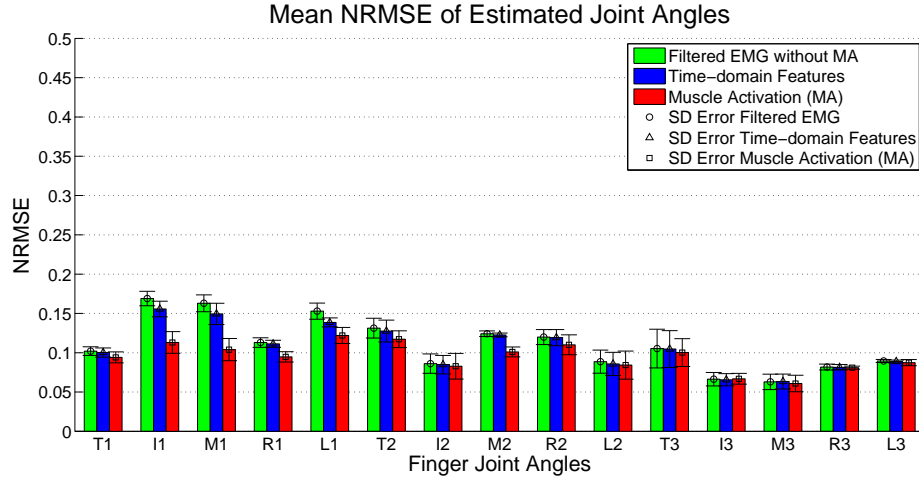


Figure 6.5: The mean normalized root-mean-square error (NRMSE) of the predicted and measured joint angles, across three different inputs used: filtered sEMG, time-domain features, and muscle activation inputs. The x-axis labels represent the same corresponding finger joint angles assignment as in Figure 6.4.

correlation coefficients in all the predicted finger joint angles and lesser mean root-mean-square errors (less than 15%), with all p-values across all the finger joint angles less than 0.05.

For the MCP joint angles, correlation coefficients of above 0.8 were achievable. This is consistent and can even go above 0.9 when the movement condition is constrained (e.g. in predicting only individual finger as opposed to simultaneous and multiple fingers, or in estimating only periodic movements and constant velocity movements as opposed to free nonperiodic ones).

6.3. Comparison Between ANN and GP Regression

Figure 6.6 shows the global performance of the predictors that we used, plotting the average RMSE of all the joint angles when the number of training samples was varied. It is interesting to see that as few as 200 samples for GP can give almost equal or even better performance as when more than 1800 samples are used to train a neural network. We also show a local test sample prediction of the MCP finger joint angles, trained with 214 samples, with both prediction from the neural network and GP superimposed in

Figure 6.7, and trained with 2134 samples in Figure 6.8.

GP gives better prediction of the joint angles using very few training samples. However we should point out that, though GP can handle missing data more readily than neural networks, the computation time becomes significantly higher in the former as the size of the training sample increases. Also, because each output joint angle was modelled independently in the Gaussian process. Using a neural network is not only fast but gives reasonable accuracy and is best suited for such simultaneous finger joint angle estimation from sEMG signals. It took about 10 times longer to train the GP than the neural network.

Despite the initial work on the use of GP, it is promising in giving better prediction in this EMG to finger joint angle prediction setting using fewer training samples. A better model where the output joint angle can be simultaneously predicted using a single or fewer models would be desirable and may exceed the performance of that using the neural network. Choosing the covariance and mean function that can best model the relationship between the EMG and finger joint angles can also improve estimation.

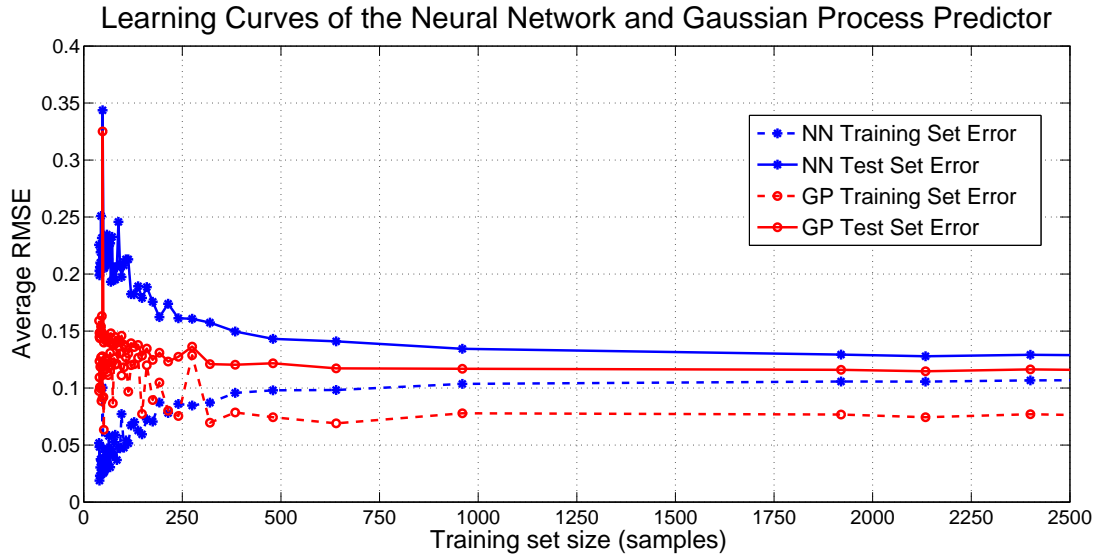


Figure 6.6: Learning curves of the neural network and Gaussian process regressor. The number of training samples were varied while the number of test data samples remained fixed.

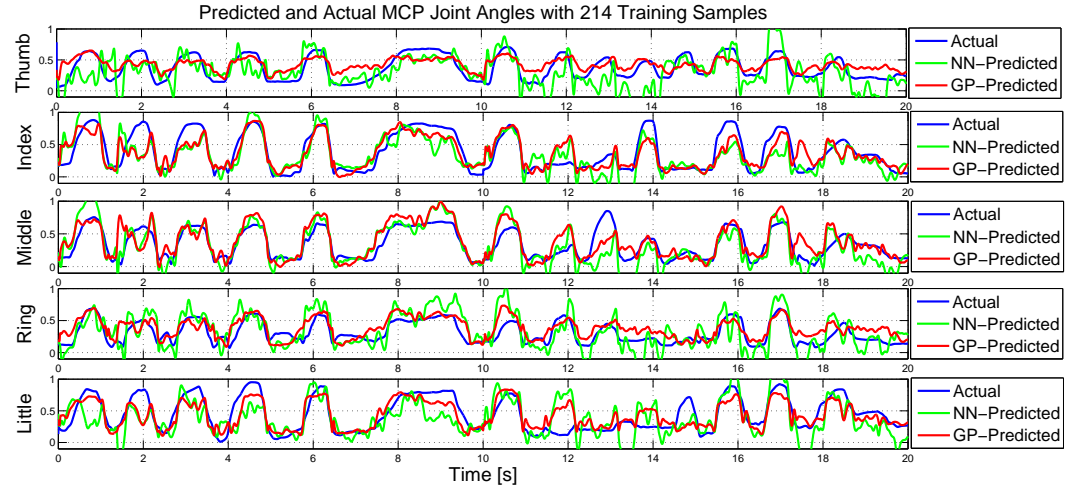


Figure 6.7: The actual and predicted MCP joint angles from the ANN and GP Regressor trained with 214 Samples.

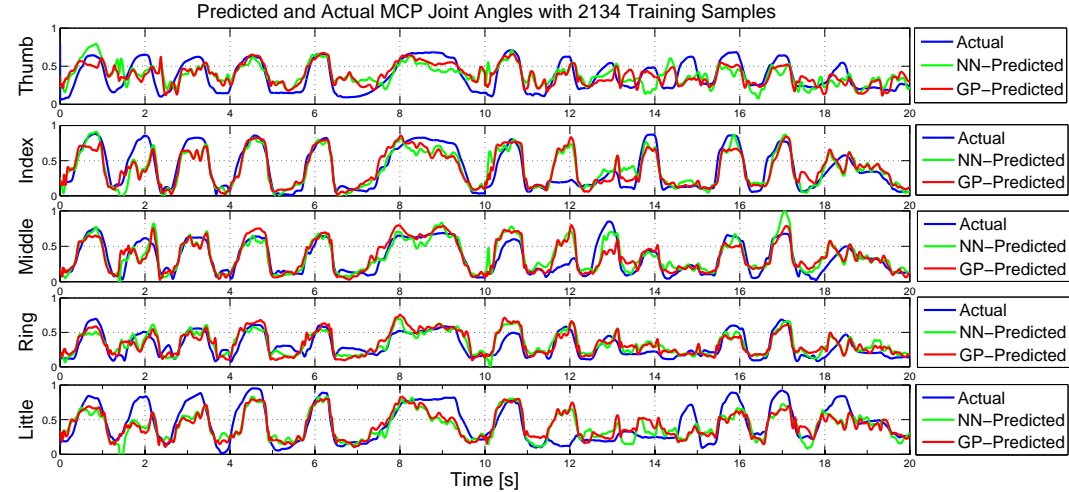


Figure 6.8: The actual and predicted finger MCP joint angles from the ANN and GP Regressor trained with 2134 Samples.

6.4. Dimensionality Analysis for Hand/Finger Movements

One issue in the method and earlier results that we presented is that we are trying to predict 15 finger joint angles in the flexion and extension plane independently using information from eight sEMG signals in the forearm. Intuitively, this can be seen as

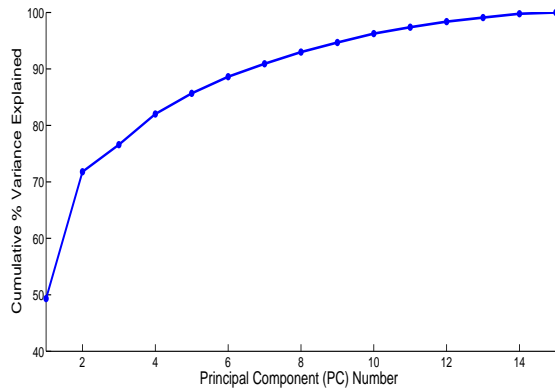
an ill-posed problem as there are more outputs than the number of inputs. However, a dimensionality analysis on the hand/finger movement data suggests that the effective dimensions is less than the total degrees of freedom (DOF) available anatomically on the hand. In other words, anatomically, the five fingers in a hand comprises a total of 15 joints, which approximately gives about 20 DOFs [34]. However, the extent to which each of these DOFs is independently controlled during movement is unknown. Previous studies suggest that hand movements have fewer dimensions than the maximum mainly due to mechanical constraints in the structure of the hand and the existence of synergies [34, 35].

In this study, a *Principal Component Analysis* (PCA) was applied on our finger joint angle dataset which spans a 15-dimensional space. PCA was performed not only on the joint angular position data, but also on the joint angular velocities data because these are said to be more closely related to the motor command's driving moment [36].

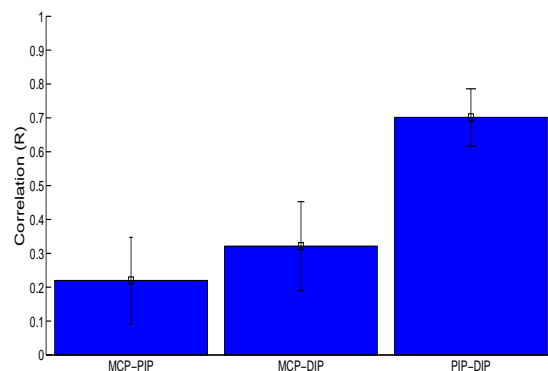
Results shown in Figure 6.9 and Figure 6.10 show that the first 4 to 6 principal components explains the vast majority of the variance in hand posture. The result of the PCA analysis on the angular positions and the angular velocity were similar. This similarity confirms from previous studies that almost certainly human movements are discrete with bell-shaped velocity profiles, which would tend to correlate variance in position with variance in velocity [34]. In the previous studies, the existence of PCs has been used to argue for synergistic control of the hands [34, 36].

Also by doing correlation analysis of finger joints, the results suggests and confirms that there is high correlations between angles of the major points of the fingers. Figure 6.9b confirms that there is high correlation in the PIP and DIP joint angles in the same finger. While joint angles in adjacent fingers are highly correlated as shown in Figure 6.9c and Figure 6.10c. These correlation results verifies our knowledge about coupled hand movements, where it is difficult for human subjects to move one digit without some degree of involuntary movement at one or more of the other digits.

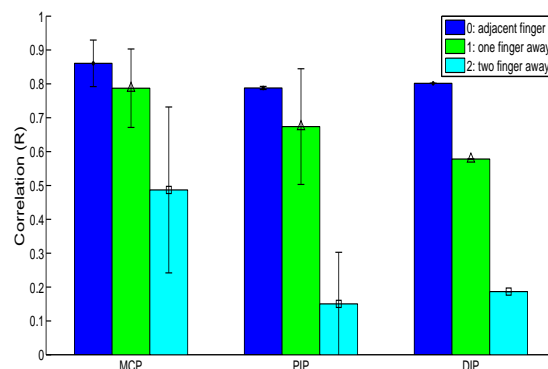
Overall, the PCA dimensionality and correlation analysis of hand movements suggest that the effective dimensionality of hand movements is indeed lower than the theoretical number of DOFs possible. These results not only suggest dimensionality reduction but may also be evidence for the existence of motor synergies in the control of the hand.



(a) Cumulative variance by PCA on the joint angular data

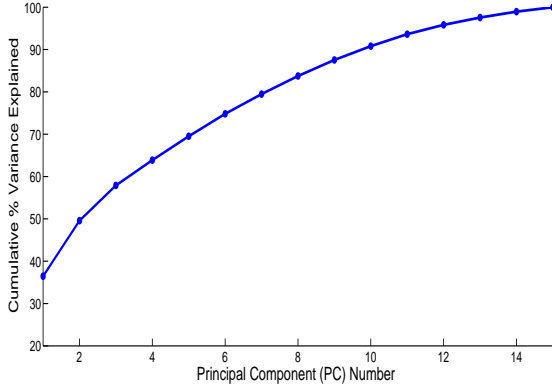


(b) Correlation between joints within the same finger

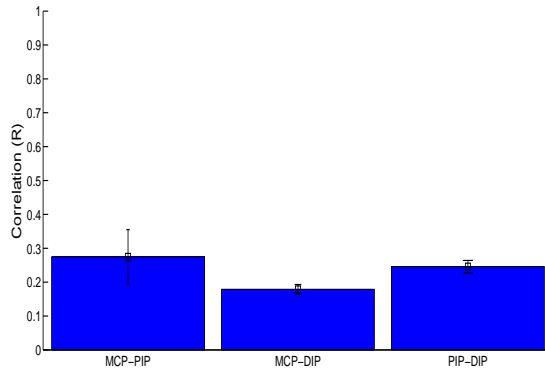


(c) Correlation between the joints across fingers

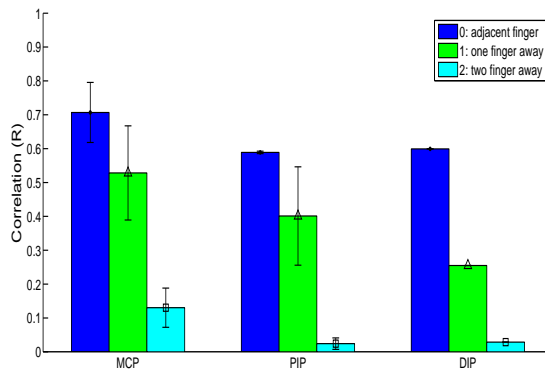
Figure 6.9: PCA on the joint angle data and correlations between finger joints.



(a) Cumulative variance by PCA on the joint velocity data



(b) Correlation of velocities between joints within the same finger



(c) Correlation of velocities between the joints across fingers

Figure 6.10: PCA on the joint velocity data and correlations between finger joints.

Chapter 7

Conclusion

This thesis presents an alternative and improved method in estimating finger joint angles using a muscle activation model that parameterizes electromechanical delay (EMD), which has been observed by numerous investigators. Automatically determining this delay improves the synchronization of sEMG signal and the finger joint angle, thus, providing better estimation. We have shown in this work that our results are comparable, if not better than previous studies in terms of using fewer inputs and fewer parameters while estimating more finger joint angles simultaneously.

Overall, our current method captures the general trend of the finger movement and is able to predict multiple finger joint angles with reasonable accuracies using muscle activation features. Though additional information from a reliable biomechanical model that can relate the PIP and DIP angles to the MCP angle may improve estimation performance. Using artificial neural network can offer a black-box type of predictor, which is fast and suitably reliable in a supervised learning setting of using EMG signals to predict finger joint angles. It is also very promising to consider a nonparametric Bayesian approach using a Gaussian Process regressor, however, a suitable covariance and mean function must be determined and modelled for applications using sEMG signals.

Given that fine hand movement is complex, future work can include investigating other factors such as finger forces and different muscle activation patterns related to doing skillful tasks involving the hands. In this thesis, high correlations between finger joints have been observed. This is because the selected tasks were limited to freely moving fingers. However, in doing more specific and refined tasks, such as in

manipulation of small objects, this may not be the case. Studies have shown that in some three-finger cooperative tasks, such as in manipulating a small coin, the thumb and middle finger are independently active, while the index finger is entirely passive throughout the manipulation task [37]. For freely moving fingers, we have predicted joint angles accurately. However, for other complex manipulation tasks, correlation information in fingers should be considered and taken advantage of in the use of the chosen regressor. Future extensions of this thesis should explore more complex manipulation tasks as task selection is particularly important in improving target accuracy of the joint angle prediction. Although problems such as EMD has been considered, depending on the finger manipulation tasks, EMDs may be continuously changing. Thus, this work can be extended to consider dynamically changing EMDs, specially when applied to real-time applications.

Some possible applications of our work includes using our proposed method in the control of robotic hand prostheses and in robotic finger exoskeletons, where the use of sEMG-based control strategies can smoothly give intended positions based on the patient's motor intention. We shortly illustrated in Appendix D, how our proposed method was used to predict a user's index finger joint angle and feed the predicted angles to control a customized finger exoskeleton. This is but only a step closer to reaching our ultimate goal of providing hand and finger rehabilitation using a sEMG-based control strategy for assistive aids. In the future, it would also be wise to explore other control strategies, such as an assist-as-needed type of control, which is not only suitable for rehabilitation but can potentially allow maximum functional recovery through the use of robotic assistive devices.

Acknowledgements

First of all, I would like to express my sincerest gratitude to my advisors, Professor Kazushi Ikeda and Associate Professor Tomohiro Shibata who have continuously guided and supported me in my study in NAIST.

To Professor Ikeda, who welcomed me as an intern in 2009, and took me in as a student in his lab. His guidance and generosity have allowed me to accomplish one of my lifelong dreams, which is to complete my study in Japan. I am humbled and honored to be a part of the Mathematical Informatics Laboratory in NAIST.

To Associate Professor Shibata, my adviser, to whom I will be forever grateful for his guidance and inspiration to make me always strive harder and bring out the best in the work that I do. His words and encouragement have always inspired me to aim high and never give up. He gave me freedom to experiment with my ideas yet at the same time was always there to guide and support me with any obstacles that came.

I am also very grateful to Assistant Professor Tomoya Tamei, who has been one of the advisors working closely with me. His patience in teaching and guiding me personally has been relentless. This thesis would not have come to fruition without his mentorship and constant support.

To Assistant Professors Takatomi Kubo, Hiroyuki Funaya, and Kazuho Watanabe, thank you very much for all your guidance and valuable inputs. It was because of their help that I was able to overcome many difficulties in this research. Special thanks to Assistant Professor Kubo, who gave me indispensable advices and many wonderful inputs and perspective on my research.

In the completion of this thesis, many people have helped me. I would like to thank Lynn who has always been hugely supportive and has always been by my side. To my parents and family, who have continuously poured me with support and encouragements and have been a valuable part of every chapter in my life.

I am very fortunate to have worked with wonderful people in the Mathematical Informatics Lab. My labmates have made my stay in NAIST truly memorable and worthwhile. I would like to specially thank my Senpais Chihiro Obayashi, Akihiro Nakamura, Zujie Zhang and Mauricio Burdelis who have helped me a lot in my stay in the lab and as well as in my stay in Japan.

To the wonderful Filipino and International community, thank you for the friendship and good times, your presence made my stay in NAIST enjoyable and memorable.

To my thesis panelists, Professor Ikeda, Professor Ogasawara, Associate Professor Shibata and Assistant Professor Tamei, thank you once again for your time, patience, and valuable inputs.

Finally, I would like to thank the Japan Government Scholarship Program and the Grant-in-Aid for Scientific Research from Japan Society for the Promotion of Science, for the support in my education and research. Without the Japan Government Scholarship, my dream of studying in Japan would never have came true. Thank you for this valuable opportunity.

References

- [1] B. Dallon and Y. Matsuoka, “Prosthetics, exoskeletons, and rehabilitation,” in *IEEE Robotics and Automation Magazine*, 2007.
- [2] O. Fukuda, T. Tsuji, M. Kaneko, and A. Otsuka, “A human-assisting manipulator teleoperated by emg signals and arm motions,” *IEEE Transactions on Robotics and Automation*, 2003.
- [3] K. Tong, X. Hu, K. Fung, X. Wei, W. Rong, and E. Susanto, “An emg-driven exoskeleton hand robotic training device on chronic stroke subjects: Task training system for stroke rehabilitation,” in *IEEE International Conference on Rehabilitation Robotics (ICORR)*, 2011.
- [4] S. Saponas, D. Tan, D. Morris, R. Balakrishnan, J. Turner, and J. Landay, “Enabling always-available input with muscle-computer interfaces,” in *ACM UIST*, 2009.
- [5] P. Afshar and Y. Matsuoka, “Neural-based control of a robotic hand: evidence for distinct muscle strategies,” in *Proc. 2004 IEEE International Conference on Robotics and Automation*, vol. 5, pp. 4633–4638, IEEE, April 2004.
- [6] N. Shrirao, N. Reddy, and D. Kosuri, “Neural network committees for finger joint angle estimation from surface emg signals,” *Biomedical Engineering Online*, vol. 8(2), pp. 1–11, 2009.
- [7] R. Smith, F. Tenore, D. Huberdeau, R. Etienne-Cummings, and N. Thakor, “Continuous decoding of finger position from surface emg signals for the control of powered prostheses,” in *Proc. 30th Annual International IEEE EMBS Conference*, pp. 197–200, IEEE, August 2008.
- [8] M. Hioki and H. Kawasaki, “Estimation of finger joint angles from semg using a neural network including time delay factor and recurrent structure,” *International Scholarly Research Network (ISRN) Rehabilitation*, 2012.
- [9] N. Pratt, *Anatomy and Kinesiology of the Hand*, vol. 1. Elsevier Mosby Philadelphia PA, 6 ed., 2011.

- [10] B. Dubuc, “MS Windows NT the brain from top to bottom.” <http://thebrain.mcgill.ca>, 2002. Accessed: 20/12/2012.
- [11] “Motor unit adaptation.” <http://kin450-neurophysiology.wikispaces.com/Motor+Unit+Adaptation>, 2011. Accessed: 20/12/2012.
- [12] W. Penfield and T. Rasmussen, “The cerebral cortex of man; a clinical study of localization of function.,” 1950.
- [13] M. Zecca, S. Micera, M. Carrozza, and P. Dario, “Control of multifunctional prosthetic hands by processing the electromyographic signal,” *Critical Reviews in Biomedical Engineering*, vol. 30, pp. 459–485, 2002.
- [14] J. Basmajian and C. De Luca, *Muscles Alive - Their Function Revealed by Electromyography*, vol. 4. Williams and Wilkins, Baltimore, MD, 1985.
- [15] P. Konrad, “The abc of emg - a practical introduction to kinesiological electromyography,” 13430 N. Scottsdale Rd., Suite 104, Scottsdale, AZ 85254, April 2005.
- [16] B. Feinstein, B. Lindegard, E. Nyman, and G. Wohlfart, “Morphological studies of motor units in normal human muscles,” *Acta Anat*, vol. 23, pp. 127–142, 1955.
- [17] G. Lisi, “The study of the electromyographic signal for the control of a prosthetic hand,” 2010.
- [18] T. Buchanan, D. Lloyd, K. Manal, and T. Besier, “Neuromusculoskeletal modeling: Estimation of muscle forces & joint moments and movements from measurements of neural command,” *Journal of Applied Biomechanics*, vol. 20(4), pp. 367–395, November 2004.
- [19] G. Saridis and T. Gootee, “Emg pattern recognition for a prosthetic arm,” *IEEE Transaction on Biomedical Engineering*, vol. 29, pp. 403–412, 1982.
- [20] K. Kiguchi, T. Tanaka, and F. Toshio, “Neuro-fuzzy control of a robotic exoskeleton with emg signals,” *IEEE Transactions on Fuzzy System*, vol. 12(4), pp. 481–490, 2004.

- [21] H. Huang and C. Chen, “Development of a myoelectric discrimination system for a multi-degree prosthetic hand,” in *Proceeding of the 1999 IEEE International Conference on Robotics and Automation*, 1999.
- [22] K. Englehart and B. Hudgins, “A robust, real-time control scheme for multi-function myoelectric control,” *IEEE Transactions on Biomedical Engineering*, vol. 50, pp. 848–854, 2003.
- [23] Y. Huang, K. Englehart, B. Hudgins, and A. Chan, “A gaussian mixture model based classification scheme for myoelectric control of powered upper limb prostheses,” *IEEE Transactions on Biomedical Engineering*, vol. 52, pp. 1801–1811, 2005.
- [24] J. Chu, I. Moon, and M. Mun, “A real-time pattern recognition for multifunction myoelectric hand control,” in *Proc. 2005 International Conference on Control, Automation and System*, ICCAS, June 2005.
- [25] L. Li and B. Baum, “Electromechanical delay estimated by using electromyography during cycling at different pedaling frequencies,” *Journal of Electromyography and Kinesiology*, 2004.
- [26] P. Vint, S. McLean, and G. Harron, “Electromechanical delay in isometric actions initiated from nonresting levels,” *Medical and Science in Sports and Exercises*, 2001.
- [27] K. Manal, R. Gonzalez, D. Lloyd, and T. Buchanan, “A real-time emg-driven virtual arm,” *Computers in Biology and Medicine*, vol. 32(1), pp. 25–36, 2002.
- [28] B. C. Csáji, “Approximation with artificial neural networks,” *Faculty of Sciences, Etvs Lornd University, Hungary*, 2001.
- [29] C. Bishop, *Pattern recognition and machine learning*, vol. 4. Springer New York, 2006.
- [30] M. Frean, M. Lilley, and P. Boyle, “Implementing gaussian process inference with neural networks,” *International Journal of Neural Systems*, vol. 16, pp. 321–327, 2006.

- [31] C. Rasmussen and C. Williams, *Gaussian Processes for Machine Learning*. MIT Press, Cambridge, MA, USA, 2006.
- [32] M. Ebden, “Gaussian processes for regression: A quick introduction,” 2008.
- [33] C. Rasmussen and H. Nickisch, “Gaussian processes regression and classification toolbox version 3.1.” <http://gaussianprocess.org/gpml/code>, September 2010. Accessed: 22/12/2012.
- [34] J. Ingram, K. Kording, I. Howard, and D. Wolpert, “The statistics of natural hand movements,” *Experimental Brain Research*, vol. 188(2), pp. 223–236, 2008.
- [35] A. d’Avella, P. Saltiel, and E. Bizzi, “Comnination of muscle synergies in the construction of a natural motor behavior,” *Nature Neuroscience*, vol. 6, pp. 300–308, 2003.
- [36] E. Todorov and Z. Ghahramani, “Analysis of the synergies underlying complex hand manipulation,” in *26th Annual International Conference of the IEEE EMBS*, IEEE, 2004.
- [37] M. F. Orlando, A. Dutta, A. Saxena, L. Behera, T. Tamei, and T. Shibata, “Manipulability analysis of human thumb, index and middle fingers in cooperative 3d rotational movements of a small object,” *Robotica*, vol. FirstView, pp. 1–13, 2 2013.
- [38] J. Ngeo, T. Tamei, and T. Shibata, “Continuous estimation of finger joint angles using muscle activation inputs from surface emg signals,” in *34th Annual International Conference of the IEEE EMBS*, pp. 2756–2759, IEEE, 2012.
- [39] “Biomechanics of the hand.” <http://www.bioeng.nus.edu.sg/comppbiolab/projects/hand-biomechanics.html>, November 2007. Accessed: 20/12/2012.
- [40] J. Ngeo, T. Tamei, and T. Shibata, “Continuous estimation of finger joint angles using inputs from an emg-to-muscle activation model,” in *MBE-IEICE Technical Report*, vol. 112, pp. 17–22, 2012.

- [41] T. Tamei and T. Shibata, “Fast reinforcement learning for three-dimensional kinetic human-robot cooperation with an emg-to-activation model,” *Advance Robotics*, vol. 25, pp. 563–580, 2011.
- [42] C. Antfolk, C. Cipriani, M. Controzzi, M. Carrozza, G. Lundborg, B. Rosen, and F. Sebelius, “Using emg for real-time prediction of joint angles to control a prosthetic hand equipped with a sensory feedback system,” *Journal of Medical and Biological Engineering*, vol. 30(6), pp. 399–406, 2010.
- [43] F. Tenore, A. Ramos, A. Fahmy, S. Acharya, R. Etienne-Cummings, and N. Thakor, “Decoding of individuated finger movements using surface electromyography,” *IEEE Transactions on Biomedical Engineering*, vol. 56, pp. 1427–1434, 2009.
- [44] C. Choi, S. Kwon, W. Park, H. Lee, and J. Kim, “Real-time pinch force estimation by surface electromyography using an artificial neural network,” *Medical Engineering and Physics*, vol. 32, pp. 429–436, 2010.
- [45] I. Nabney, *NETLAB: algorithms for pattern recognition, Advances in Pattern Recognition*. Springer, Berlin, 2001.
- [46] M. Hioki and H. Kawasaki, “Estimation of finger joint angles from semg using a recurrent neural network with time-delayed input vectors,” in *IEEE 11th International Conference on Rehabilitation Robotics*, pp. 289–294, IEEE, June 2009.
- [47] H. Ogino, J. Arita, and T. Tsuji, “A wearable pointing device using emg signals,” *Journal of Robotics and Mechatronics*, 2005.
- [48] M. H. Schieber, “Muscular production in individuated finger movements: The roles of extrinsic finger muscles,” *The Journal of Neuroscience*, vol. 15(1), pp. 284–297, 1995.
- [49] I. Nabney and C. Bishop, “Netlab neural network software,” *Matlab Toolbox*, vol. 71, 2003.

Appendix

A. Prediction Performance of ANN and GP Regression

The following plots show the mean correlation coefficient as well as the mean normalized root mean square error (NRMSE) of all the estimated joint angles obtained from a 5-fold cross validation. Using Gaussian Process with basic assumptions of the covariance and mean function can outperform and give better estimation results. It can be observe however that the NRMSE values are much larger than that obtained in Figure 6.5. The main reason for this is that in order to accommodate the use of GP, where it is much computationally intensive than ANN, significantly fewer training samples were used.

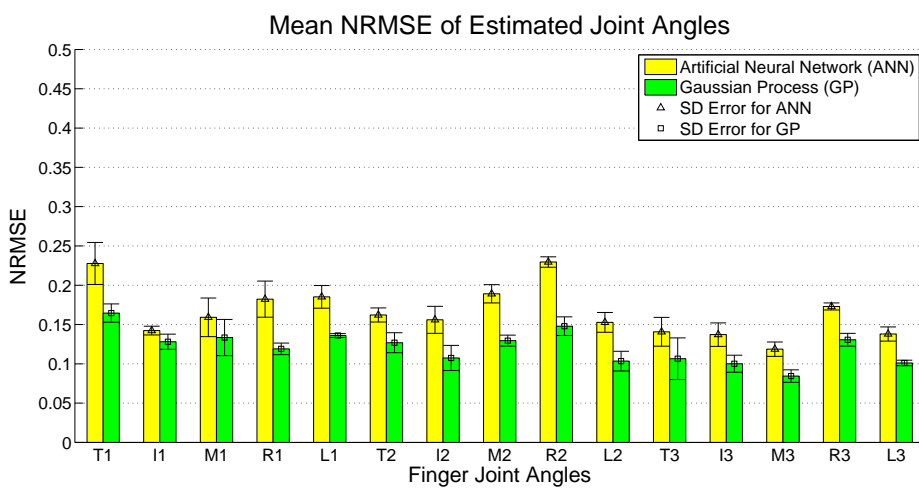
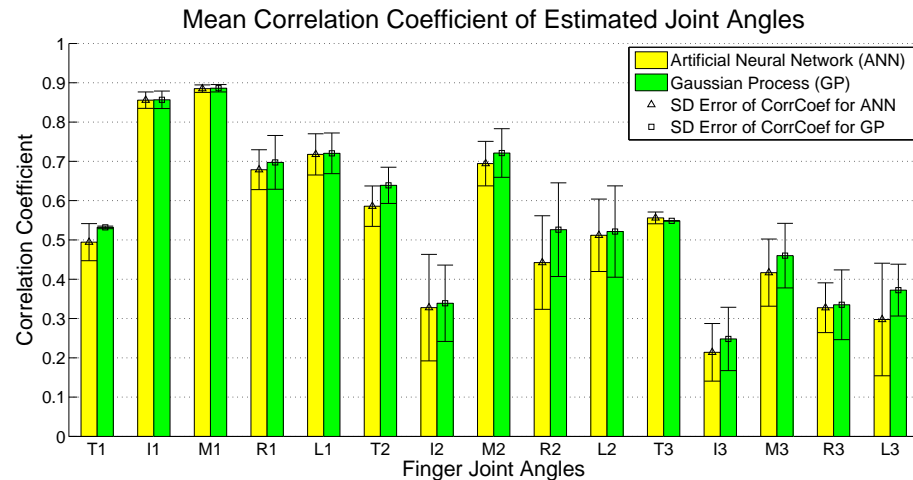


Figure 7.1: The mean correlation coefficient and the mean NRMSE of the predicted and measured finger joint angles, across the two different regression methods are compared. The x-axis letter labels represent the thumb, index, middle, ring, and little finger, while the numbers 1, 2, and 3 are the MCP, PIP, and DIP angles, respectively.

B. Processed EMG Used in the Sample Test Result

Here we show the rectified and normalized EMG signal obtained in the test data shown in Figure 6.7 and 6.8 in Section 6.3. The EMG signals were low-pass filtered, using a zero-phase Butterworth filter with cut-off frequency of 4 Hz, and was then converted using a suitable muscle activation model. In this particular test data, the parameters obtained for the muscle activation mode were: $A = -3$, $d = 0.045$, $\gamma_1 = \gamma_2 = -0.9539$. The labels on the y-axis of the plots correspond to the target EMG channels which is listed in Table 5.1.

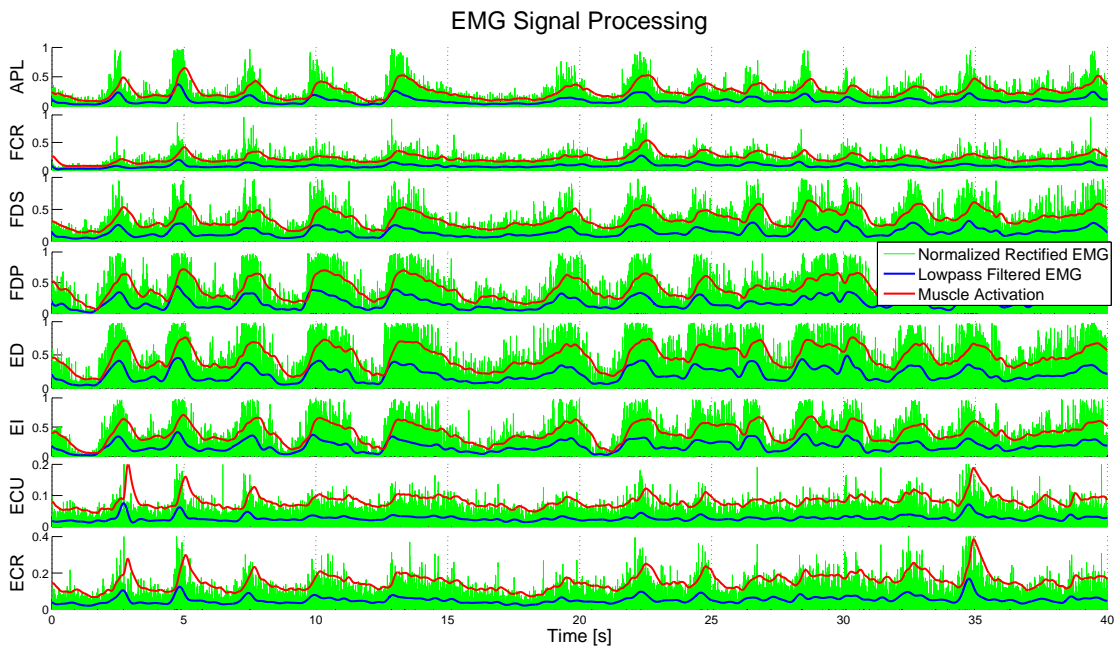


Figure 7.2: Muscle activations are transformed from preprocessed EMG signal using obtained parameters.

C. PIP and DIP Joint Angles Prediction Results

The following plots show the corresponding predicted PIP and DIP joint angles discussed earlier in Section 6.3. In that section, only the MCP joint angle prediction of a sample test trial was shown. Here, we show the corresponding PIP joint angle predicted results of all 5 fingers for that trial trained with 214 and 2134 samples. The y-axis values which ranges from 0 to 1 are normalized values with respect to Table 5.2

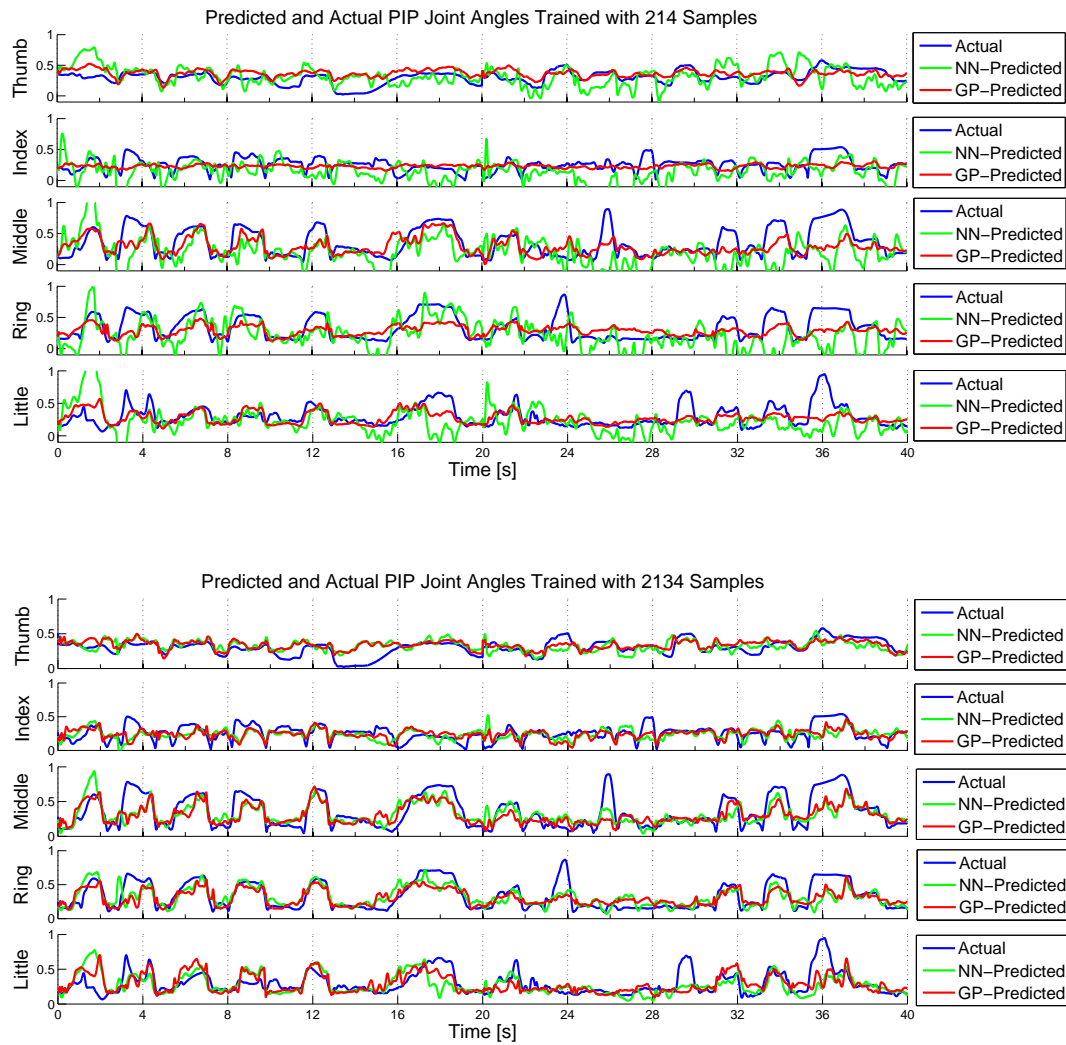


Figure 7.3: The actual and predicted PIP joint angles from the ANN and GP Regressors at two different training sample size.

In the following plots, we show the corresponding DIP joint angle predicted results using ANN and GP regressor of all 5 fingers for the same trial trained with 214 and 2134 samples.

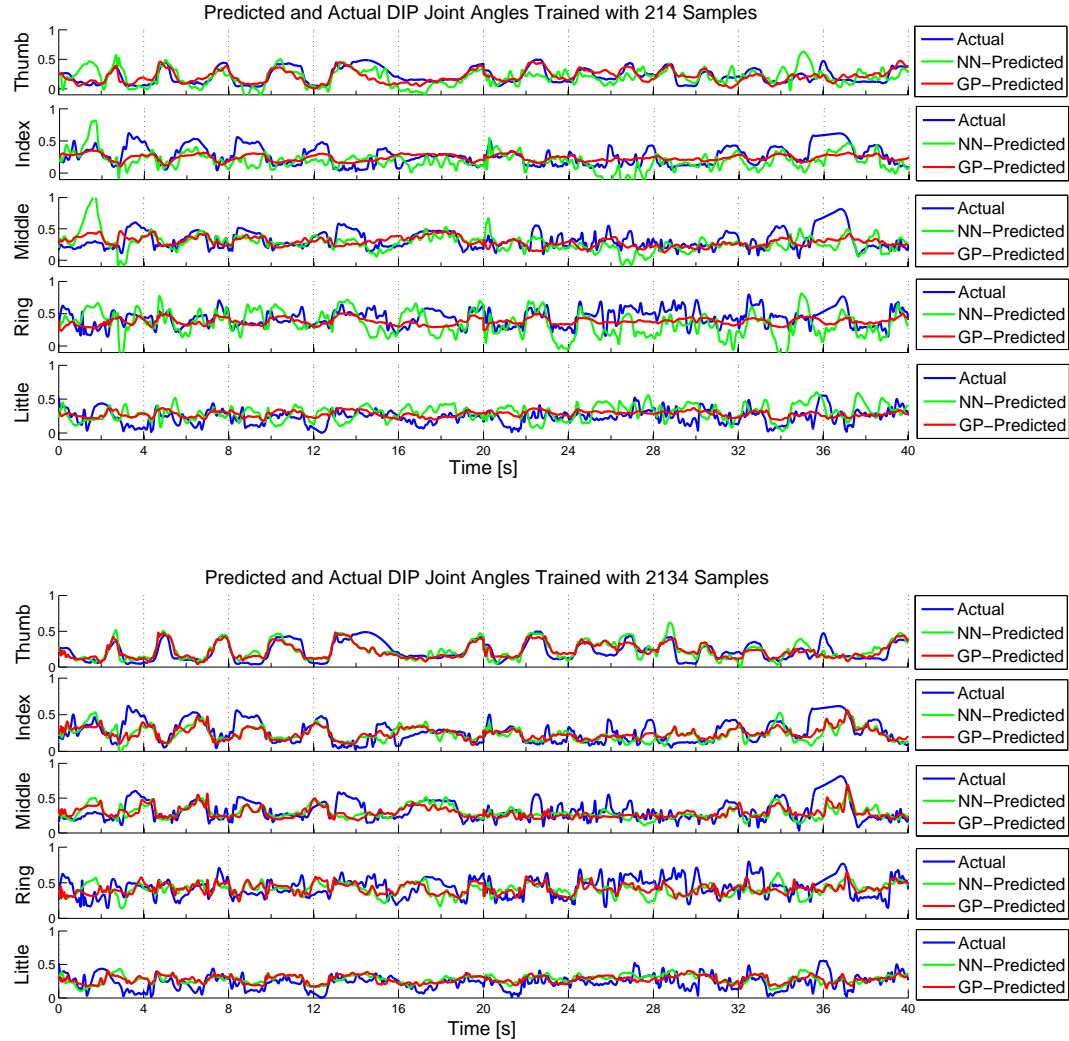


Figure 7.4: The actual and predicted DIP joint angles from the ANN and GP Regressors at two different training sample size.

D. Application: Control of a Finger Exoskeleton

Here, we show one sample application where sEMG signals were used to predict and control a custom-made index finger exoskeleton. A subject was asked to move his left index finger in the flexion and extension plane while the right index finger was actuated by the exoskeleton using EMG inputs from the left side (Figure 7.5a). No exerted EMG effort came from the right finger to show that it was indeed assisted by the exoskeleton (Figure 7.5b). Finally, the joint angle test prediction result is shown in Figure 7.5d, when the EMG was transformed into its muscle activation and used as input to predict the index finger joint angle. The blue plot shows the measured joint angle obtained from the left index finger, while the red plot shows the predicted joint angle from the regressor. The green plot shows the actuated motion of the finger exoskeleton on the right index finger.

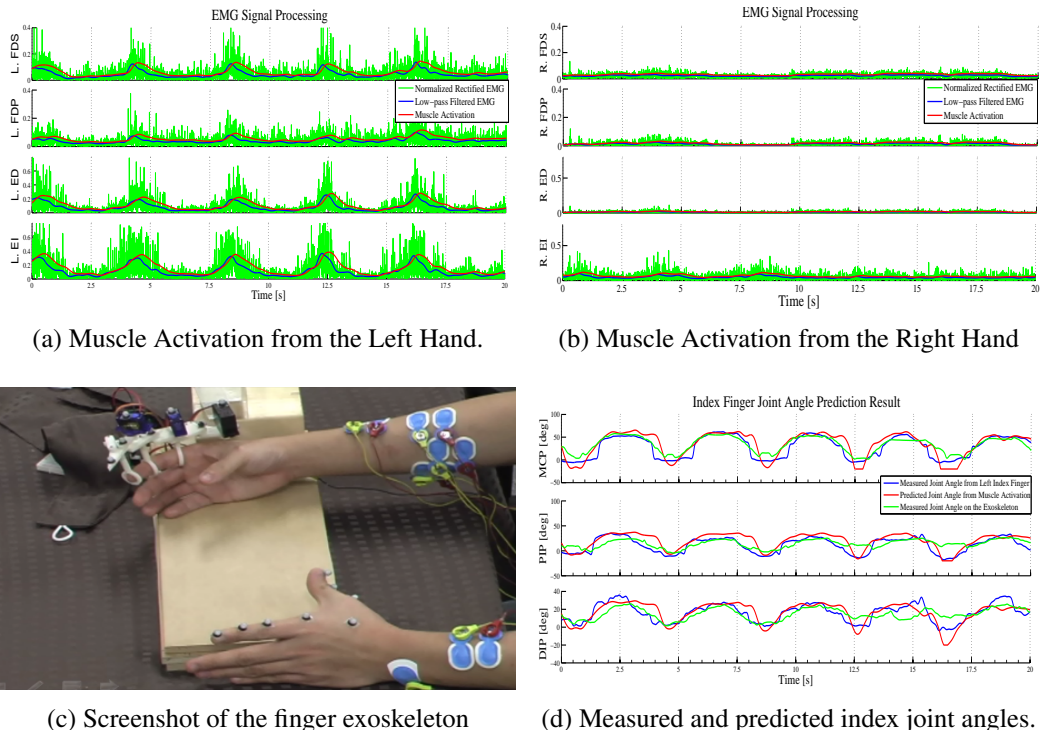


Figure 7.5: An application showing an sEMG-based control of an index finger exoskeleton. The recorded sEMG on both left and right hand are shown and the robot was controlled with input commands coming from the predicted joint angles.